THE PARTICLE-HOLE MODEL APPLIED TO DIPOLE EXCITED STATES OF CARBON AND SILICON

A Thesis

Submitted to the Faculty of Graduate Studies

in Partial Fulfilment of the Requirements

for the Degree of

Master of Arts

in the Department of Physics

University of Saskatchewan

by

David Alexander Hutcheon

Saskatoon, Saskatchewan

August, 1965

ABSTRACT

The particle-hole model of nuclear excited states is discussed, and a method of obtaining excited state wave functions is outlined for a simple version of the model. Expressions are given for cross sections for excitation of particle-hole states by inelastic electron scattering. Particle-hole model predictions and experimental results concerning dipole states in C^{12} and Si^{28} are given. The feasibility of using the Saskatchewan electron accelerator to study these states is considered. The nature and size of background to be expected is discussed in detail.

ACKNOWLEDGMENTS

The author would like to thank Dr. J.D. King for suggesting this topic and Dr. J.A. Moore for his guidance in the writing of this thesis.

The author is indebted to visitors and students at the Saskatchewan Accelerator Laboratory for many useful and illuminating discussions on various aspects of the thesis. The material in Appendix C is based upon work on dead time corrections which was done by Dr. D. McArthur and the author.

The author wishes to thank George Beer for his careful proofreading of the thesis.

The financial assistance of the National Research Council is gratefully acknowledged.

TABLE OF CONTENTS

LIST OF FIGURES

LIST OF TABLES

TABLE OF SYMBOLS

a	A destruction operator for a single particle in occupation-number representation.
$a^\dagger$	A single particle creation operator in occupation-number representation.
A	The mass number of a nucleus.
b	The radial parameter in harmonic oscillator functions.
e	The charge of an electron.
$\vec{e}$	The unit polarization vector.
E_i, E_f	Energies of incident and scattered electrons.
H	The Hamiltonian for a nucleus.
H_o	A single particle Hamiltonian containing only central and spin-orbit potentials.
H'	The interaction Hamiltonian for a nucleus and an electron.
$\vec{J}_N$	The nuclear current density operator.
$j_\lambda(qr)$	A spherical Bessel function.
J_i	The total angular momentum of the initial nuclear state.
$k_i = E_i/\hbar c$ $k_f = E_f/\hbar c$	Wave numbers of incident and scattered electrons.
m	The rest mass of an electron.
M	The rest mass of a nucleon.
$\vec{p}$	The single particle momentum operator.
$\hbar q$	The three-momentum transferred by the electron in scattering.
$R_{n\ell}$	The radial part of a single particle wave function.
$V = H - H_o$	The residual interaction between nucleons.
Y_λ^m	A spherical harmonic function.
$\mathcal{Y}_{\lambda\lambda'}^{M} = \sum_{mm'} (\lambda' m 1 m' \mid \lambda M) Y_{\lambda'}^{m} e_{m'}$	A vector spherical harmonic.
$\alpha, \beta, \gamma, \ldots$	Labels for particle states in the shell model.
$\bar{\alpha}, \bar{\beta}, \bar{\gamma}, \ldots$	Labels for hole states in the shell model.
n	Principal quantum number minus orbital angular momentum quantum number.

γ The gyromagnetic ratio: for protons $\gamma_p = 2.79$; for neutrons $\gamma_n = -1.91$.

ε The effective charge: for protons $\varepsilon_p = 1$; for neutrons $\varepsilon_n = 0$.

λ The multipolarity of a nuclear transition.

$\lambda_N = \frac{\hbar}{Mc} = 0.210\,\text{fm}$ The reduced Compton wave length of a nucleon.

$\vec{\mu}_N$ The nuclear magnetization density operator.

$\vec{\sigma}$ A Pauli spin operator.

ρ_N The charge density operator of a nucleus.

τ_3 The third component of the isotopic spin operator.

$\tau_{\frac{1}{2}}^{m_t}$ An isotopic spin eigenfuction: for a proton $m_t = \frac{1}{2}$; for a neutron $m_t = -\frac{1}{2}$.

θ The scattering angle of an electron in the laboratory system.

$\chi_{\frac{1}{2}}^{m_s}$ A spin eigenfunction for a nucleon.

$| \; \rangle$ Occupation-number representation of a state.

$| \;)$ Coordinate representation of a state.

$|g)$ The ground state of the operator H_o for a closed-shell nucleus.

$|\ell j m) = \sum_{m_\ell m_s} (\ell m_\ell \tfrac{1}{2} m_s | j m)\, Y_\ell^{m_\ell} \chi_{\frac{1}{2}}^{m_s}$ The angular momentum part of a single particle wave function.

$|n \ell j m m_t) = R_{n\ell}\, |\ell j m)\, \tau_{\frac{1}{2}}^{m_t}$ A single particle wave function.

$[n \ell_j]$ One of the shells in a shell model with central and spin-orbit forces.

$(\alpha\beta|v|\gamma\delta) = \int d\vec{x}_2 \int d\vec{x}_1\, \psi_\alpha^\dagger(\vec{x}_1)\, \psi_\beta^\dagger(x_2)\, v(\vec{x}_1, \vec{x}_2)\, \psi_\gamma(\vec{x}_2)\, \psi_\delta(\vec{x}_1)$

A matrix element of a two-body operator in coordinate representation.

$(\ell_1 m_1 \ell_2 m_2 | LM)$ A Clebsch-Gordan vector-coupling coefficient.

$\begin{pmatrix} j_1 & j_2 & j_3 \\ m_1 & m_2 & m_3 \end{pmatrix}$ A Wigner 3-j symbol.

$\begin{Bmatrix} j_1 & j_2 & j_3 \\ j_4 & j_5 & j_6 \end{Bmatrix}$ A Wigner 6-j symbol.

$\begin{Bmatrix} j_1 & j_2 & j_{12} \\ j_3 & j_4 & j_{34} \\ j_{13} & j_{24} & J \end{Bmatrix}$ A Wigner 9-j symbol.

Chapter 1

INTRODUCTION

One important branch of nuclear physics is the study of excited states of nuclei. From a study of the parities, angular momenta, excitation energies, lifetimes, and decay modes of excited states, much information can be gained concerning the interaction between nucleons.

The inelastic scattering of high-energy electrons is a useful method of exciting nuclei. It has two advantages over excitation by a bremsstrahlung beam: the energy transferred to the nucleus may be determined more exactly; and the momentum and energy transfer may be varied independently. The interaction between an electron and a nucleus remains almost entirely electromagnetic, even when the electron has enough energy to penetrate into the nucleus. This is not the case when protons or heavy ions are the projectiles. Since the internucleon force is not as well known as the electromagnetic force, the interpretation of electron scattering experiments may be subject to less uncertainty than experiments in which the probe particles are nucleons or ions.

If the interaction can be treated in first Born approximation, the transition probability per unit time for scattering of an electron can be written

$$\frac{dW}{dt} = \frac{2\pi}{\hbar} |(F|H'|I)|^2 \rho(E_f), \tag{1.1}$$

where $|I)$ and $|F)$ are the initial and final states of the nucleus-electron system, H' is the interaction between electron and nucleus, and $\rho(E_f)$ is the density of final energy states. It is possible to reduce this expression to one in which the matrix element involves only the initial and final states of the nucleus. One can insert the wave-functions given by a nuclear model and obtain a value for the scattering cross section. Thus, measurements of electron scattering cross sections provide one check on the validity of a model which is claimed to describe excited states of nuclei.

The experimental procedure is to measure scattering cross sections as a function of scattering angle, energy of incident electrons, and energy transfer. Electrons may lose energy, not only by inelastic scattering from nuclei, but also by such processes as radiation of a photon during scattering, or ionization losses in the target. It is necessary to correct experimentally measured cross sections for such effects before comparing them with the predictions of theories.

The particle-hole model, a special case of the shell model applicable to closed-shell nuclei, has recently had some success in explaining excited states of nuclei, particularly the giant dipole resonances. The model is unable to explain many of the details of recent (γ,p) and (p,γ) experiments on closed-shell nuclei, yet it remains a popular model in the interpretation of inelastic electron scattering experiments. One of the chief advantages of electron scattering is that the cross section for excitation of a level may be measured for different values of momentum transfer. Therefore, a desirable model is one which makes predictions about cross section as a function of momentum transfer. Since the particle-hole model does this quite well and the calculations are relatively easy, many of the results of inelastic electron scattering of the past three years have been compared with the particle-hole model.

The first part of this thesis contains a description of the particle-hole model and an outline of the procedure for calculating inelastic electron scattering cross sections. It is intended that this will serve as a brief introduction to the subject. At the same time, it is hoped that there is enough detailed information to permit the reader to do particle-hole model calculations without extensive reading of the literature. The second section of the thesis considers the possibility of checking certain particle-hole model predictions, using the facilities of the University of Saskatchewan electron

accelerator laboratory. The expected causes of background are discussed in detail. Previous work on dipole excited states of C^{12}, O^{16}, and Si^{28} is reviewed, then particular cases of C^{12} and Si^{28} are considered more carefully. On the basis of particle-hole model predictions, it is concluded that it would be useful to use the Saskatchewan linac facilities to study C^{12} excited states around 35 MeV excitation energy, and Si^{28} states in the region 15 MeV to 25 MeV.

Chapter 2

THE PARTICLE-HOLE MODEL OF NUCLEAR EXCITED STATES

A central problem of nuclear physics is that of the quantum mechanical treatment of a system containing many strongly-interacting particles. There are two main difficulties which thus far have made it impossible to obtain exact nuclear wave functions: there is yet no exact description of the nucleon nucleon interaction; and present-day mathematical techniques cannot readily be applied to systems containing a large number of strongly-interacting particles. In order to explain the more prominent features of experimental results, physicists have assumed certain relatively simple models for the atomic nucleus. When a simple model ceases to explain experimental results in a satisfactory manner, it is either improved or abandoned in favor of a better model.

§1 The Shell Model of the Nucleus

Amongst the many nuclear models is a group that could be called shell models of the nucleus. The assumption common to the group is that nucleons move almost independently of one another in the nucleus. In the simplest model the force which a nucleon experiences due to the other nucleons is assumed to be equivalent to a central force. The wave function of the nucleus is simply the antisymmetrized product of individual nucleon wave functions. Because we have a central potential, the nucleon wave functions are eigenfunctions of orbital angular momentum and of its component along some preferred axis. Nucleons tend to occupy the states of lowest energy, just as atomic electrons do. In the case of atomic electrons, a system in which all energy levels are either completely occupied or completely unoccupied is especially stable. One would expect the same to be the case for closed-shell nuclei if the shell model is valid. In particular, there should be a discontinuity in the values of binding energy per nucleon as one moves

from a nucleus of mass A, in which a major shell is just filled, to a nucleus of mass number A + 1. Such discontinuities have been observed, occurring after the "magic" nucleon numbers of 2, 8, 20, 28, 50, 82, and 126. However, no simple potential, such as a harmonic oscillator or infinite square-well potential, can explain more than the first three magic numbers.

This inadequacy of the shell model was remedied by the introduction of a fairly strong spin-orbit force (Mayer and Jensen (1955), chapter IV). Each nucleon is assumed to experience an additional potential of the form $-V(r)\vec{l}\cdot\vec{s}$, where $\vec{l}$ and $\vec{s}$ are the orbital angular momentum and spin angular momentum, respectively, for that nucleon. For a nucleon moving in such a potential, m_l, the projection of $\vec{l}$ along the preferred axis, is not a constant of motion. The quantum numbers by which a nucleon is designated are l, j, and m, where $\vec{j} = \vec{l} + \vec{s}$ and m is the component of $\vec{j}$ in the preferred direction. Addition of a spin-orbit potential, $-V(r)\vec{l}\cdot\vec{s}$, splits an energy level for angular momentum l into two levels, $j = l + \frac{1}{2}$ and $j' = l - \frac{1}{2}$. The splitting due to the spin-orbit force causes gaps to appear between shells in such a way as to account for all seven magic numbers (Mayer and Jensen (1955) figure IV.3).

An improvement of this simple model would be to allow a weak residual interaction between nucleons, in addition to the central potential and spin-orbit potential. It can be shown (de Shalit and Talmi (1963), page 226) that the interaction of a particle with a closed shell is exactly equivalent to an interaction with a central potential. Therefore, it is reasonable to suppose that in describing many nuclear properties we need consider only particles moving outside closed shells, i.e., that closed shells can be treated as an inert core.

The effect of a residual interaction between nucleons is to mix eigenstates of the unperturbed Hamiltonian H_o. (H_o contains a central potential

and spin-orbit potential.) If the residual interaction is small, it is reasonable to suppose that there will be appreciable mixing of only a small number of the unperturbed eigenstates. If this is the case, it is still useful to use single-particle states of the form $|nljm)$. When we consider residual interaction, the energy of a system of particles in partially filled shells depends upon the manner in which the nucleon angular momenta are coupled together. Hence, excitation of a nucleus from its ground state could be explained either as promotion of a nucleon to a higher-energy shell, or as a recoupling of the nucleons within the partially filled shells. In the special case that the ground state has no partially filled shells, the problem of describing excited states is somewhat simpler: since there is only one way to couple particles of a filled shell, excitation must be by promotion of one or more particles to a shell of higher energy.

Let us consider the excitation of a nucleon from the [nlj] shell to the shell [n'l'j'] . The parity of the nucleus as a whole is equal to the product of the parities of individual nucleons. A nucleon in the [nlj] shell has parity $(-1)^{l}$. Hence, when a particle is excited from the [nlj] shell to the [n'l'j'] shell, the change in parity is given by $(-1)^{l+l'}$. In the special case that the ground state has no partially filled shells, it has total angular momentum zero and positive parity. When a nucleon is excited from the [nlj] shell to the [n'l'j'] shell, the parity of the excited state is $(-1)^{l'+l}$ and the final state angular momentum is limited by vector addition rules to $|j'-j| \leqslant J_f \leqslant j'+j$.

The behaviour of a nearly closed shell, in a way, is like that of a nearly empty shell (de Shalit and Talmi (1963), page 229). For calculation of energy differences, a shell [nlj] with 2j particles could be considered as a closed shell plus a "hole", with the hole behaving much like an [nlj]

particle. Then, the interaction of a particle excited to the $[n'l'j']$ shell with the 2j particles of the $[nlj]$ shell could be treated by considering its interaction with a closed shell plus an $[nlj]$-type hole. In this case, calculations of residual interaction involving $(2j + 1)$ particles can be simplified to a calculation involving a particle and a hole.

§2 Relationship of the Compound Nucleus Model to the Particle-Hole Models

We shall be considering giant dipole resonances, which generally begin several MeV above the nucleon emission threshold. Excited states will be described in terms of a small number of independent-particle model wave functions. It is perhaps useful to consider the relationship between this description and the compound nucleus picture of the excited states of nuclei.

The compound nucleus model was proposed to explain resonances in certain cross sections. For example, cross sections for scattering of slow neutrons often show rapid fluctuation as a function of neutron kinetic energy. These fluctuations are in the form of narrow resonances, which suggests that the reaction goes via long-lived intermediate states. It is assumed that the incident particle interacts with the nucleus and shares its energy with the nucleons, forming a compound nucleus. The motion of the nucleons in this intermediate state is exceedingly complex. The compound nucleus is considered to "forget" how it was formed, that is, the decay modes of a compound nucleus are considered to be independent of the method of formation. Decay of the intermediate state occurs when enough energy is concentrated in one nucleon to permit it to escape the nucleus. Such intermediate states would not resemble excited states of the independent-particle model; a large number of shell model states would be required to represent a compound nucleus state.

As the energy of the intermediate state increases, the average separation of resonances decreases. Increasing the energy also shortens the average lifetime of intermediate states, resulting in an increase in resonance widths. Eventually the resonance widths begin to exceed average spacing, that is, the resonances begin to overlap. For energies in the giant resonance region we expect closely spaced, strongly overlapping levels. Let us consider an excitation energy E, where the average compound nucleus level spacing is D and the average width Γ. As an example, we consider excitation from the ground state by absorption of a gamma ray of energy E, a process which has an amplitude a(E), say. According to the compound nucleus picture, we would expect appreciable excitation of levels within an energy band of width approximately Γ, centered around E. Let us suppose that the amplitude for excitation of the compound nucleus state $|i)$ is $b_i(E)$, so that $a(E) = \Sigma_i b_i(E)$. The gamma absorption cross section $\sigma(E)$ is proportional to $|a(E)|^2$. The behaviour of $\sigma(E)$ as a function of energy will depend upon the relationships of the $b_i(E)$ to one another. We may consider two limiting cases. (1) There may be no discernable phase relationships amongst the $b_i(E)$, and therefore the amplitude a(E) is the sum of approximately Γ/D quantities which we may consider as random variables. The cross section should show fluctuations (the so-called Ericson fluctuations) of width the order of Γ (Ericson (1963)). (2) There may be some phase relationship between the $b_i(E)$ which persists over an energy interval much wider than Γ, possibly an interval of more than an MeV. The compound nucleus states may be expressed in terms of simple shell model states $|\alpha)$ as $|i) = \Sigma_\alpha c_{i\alpha}|\alpha)$. Then $a(E) = \Sigma_i b_i(E) = \Sigma_i \Sigma_\alpha c_{i\alpha} d_\alpha(E)$, where $d_\alpha(E)$ is the amplitude for gamma excitation of the shell model state $|\alpha)$. For simplicity, let us assume that the phase relationship of the $|i)$ is confined to the $c_{i\alpha}$ for one particular $|\alpha)$, that is, the states $|i)$ are related

by having their projection along $|\alpha)$ not random for one of the shell model states, say the state $|\alpha')$. When we group the terms in the amplitude as $a(E) = \Sigma_\alpha\{\Sigma_i c_{i\alpha}\}d_\alpha(E)$, the coefficient of $d_{\alpha'}(E)$ will be much larger than any of the other coefficients. The cross section $\sigma(E)$ will ~~depend~~ mainly upon the form of $d_{\alpha'}(E)$. The cross section could be explained by taking the nuclear excited state to be the simple shell model state $|\alpha')$.

The work by Singh et al.(1965) indicates that both types of behaviour, incoherent as well as coherent excitation of compound nucleus states, must be considered in the giant resonance of Si^{28}. For experiments such as electron scattering, for which the widths Γ, are less than the energy resolution, there is a damping of the Ericson fluctuations. Hence electron scattering cross sections would not show the full importance of incoherent processes. The particle-hole model, to be described in the next section, attempts to describe excited states of the nucleus in terms of a few independent-particle model wave functions. It should be kept in mind that this model is nothing more than a crude representation of the nucleus, that it is useful in "explaining" only a limited range of experimental results.

Particle-hole models of varying degrees of sophistication have been used. The more complicated versions, involving a larger number of shell model wave functions, presumably are a more faithful representation of the nucleus. The particle-hole model of nuclear excited states was the result of a schematic model of Brown and Bolsterli (1959). One-particle-one-hole theory has been applied systematically to excited states of C^{12}, O^{16}, and Ca^{40} by Gillet (1962). In the simplest model, the so-called Tamm-Dancoff treatment, the ground state for a Hamiltonian containing a weak residual interaction between nucleons is taken to be the same as that for the unperturbed Hamiltonian. A better model is one which considers modifications in the ground

state which are introduced by the residual interaction. Gillet's thesis shows how to obtain particle-hole wave functions including ground state correlations using the Hartree-Fock method and using Green's functions. A further refinement of the theory, which mixes yet a larger number of shell model wave functions, is to consider two-particle-two-hole excitations. Such a model may be necessary to explain decay of the giant resonance of O^{16} (Yergin et al.(1964)). For the formation of $J = 1$, $\pi = -1$, $T = 1$ states, the Tamm-Dancoff model appears to agree with experiment just as well as the model which includes ground state correlations. Since $1^-(T = 1)$ states are the type that will be considered, only the simple Tamm-Dancoff model is used in this thesis.

§3. Simple particle-hole model of excited states of closed-shell nuclei

This section will be an outline of how particle-hole techniques can be applied to excited states of closed shell nuclei such as C^{12} or O^{16}. We are interested in describing excited states of definite parity, angular momentum, and isotopic spin. A number of states for an excited nucleon may be compatible with the requirement that the final state have a certain parity, angular momentum, and isotopic spin. To illustrate this, let us consider O^{16}.

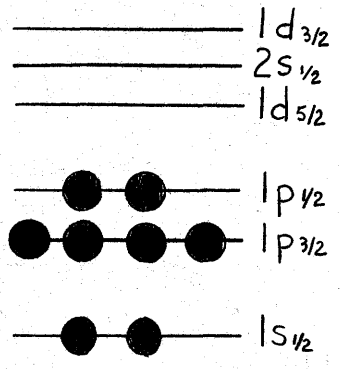

Fig. 2.1 Ground state configuration of O^{16}.

In a simple shell model, the ground state consists of 8 neutrons and 8 protons in the lowest three energy levels, as shown in Figure 2.1. The method of labelling energy levels is standard shell model notation and is explained in Elliott and Lane (1957). Neutrons and protons are assumed to fill shells independently. Suppose we are interested in

a state with angular momentum 1 and negative parity. One way of getting such a final state is to excite a nucleon from the $1p_{3/2}$ level to the $1d_{5/2}$ level. On the other hand, excitation from the $1p_{1/2}$ level to the $1d_{5/2}$ level cannot give a 1^- state, due to angular momentum addition rules.

Inclusion of a weak residual interaction V between nucleons will modify the excited states and their energies. A number of eigenstates of the unperturbed Hamiltonian H_o will have a given parity and angular momentum. An eigenstate of the perturbed Hamiltonian, $H = H_o + V$, can be represented as a linear combination of eigenstates of H_o. These eigenstates of H_o must all have the same parity and angular momentum. We further limit the number of states in the linear combination by restricting the difference in energies between the initial and final energy levels of the excited nucleon. For example, in a 1^- state of O^{16} we would consider only the five eigenstates of H_o obtained by the following single-particle excitations: $1p_{1/2} \rightarrow 1d_{3/2}$, $1p_{1/2} \rightarrow 2s_{1/2}$, $1p_{3/2} \rightarrow 1d_{3/2}$, $1p_{3/2} \rightarrow 2s_{1/2}$, and $1p_{3/2} \rightarrow 1d_{5/2}$.

Eigenstates and eigenenergies of the perturbed Hamiltonian are found by calculating matrix elements of the type $(\alpha|H|\beta)$, where $|\alpha)$ and $|\beta)$ are suitable eigenstates of H_o of the type described above, and diagonalizing the resulting matrix. If we choose one-particle states which are eigenstates of $\vec{j}^2$, then matrix elements $(\alpha|H_o|\beta)$ are non-zero only for $|\alpha) = |\beta)$. The diagonal terms $(\alpha|H_o|\alpha)$ are obtained from experimental results in the following way: Let ϵ_2 be the energy required to add to the closed-shell nucleus a nucleon in the $[n_2 l_2 j_2]$ shell. Similarly we call ϵ_1 the energy which must be added to a nucleus with a hole in the $[n_1 l_1 j_1]$ shell to produce a closed-shell nucleus in the ground state. In many cases ϵ_1 and ϵ_2 may be obtained from tables of energy levels (eg. Ajzenberg-Selove and Lauritsen (1959)). Then $(\alpha|H_o|\alpha) = \epsilon_2 - \epsilon_1$, where $|\alpha)$ is the state with a hole in the $[n_1 l_1 j_1]$ shell and a particle in the $[n_2 l_2 j_2]$ shell.

We are now left with the calculation of matrix elements $(\alpha|V|\beta)$. To avoid dealing with antisymmetrized products of single-particle wave functions (as is done by Lewis and Walecka (1964)), it is convenient to carry out the calculations using occupation-number representation of nuclear states. A system which has n_1 particles in state 1, n_2 particles in state 2, etc. may be specified by $|n_1, n_2, \ldots\rangle$. For a system such as the nucleus, which is made up of fermions, these occupation numbers are either 0 or 1. Let us define $S_j = \sum_{k=1}^{j-1} n_k$ (Schweber (1961), page 138). A destruction operator a_j may be defined by

$$a_j |n_1, n_2, \ldots n_j, \ldots\rangle = (-1)^{S_j} n_j |n_1, n_2, \ldots n_j - 1, \ldots\rangle \tag{2.1}$$

and a creation operator $a_j^\dagger$ by

$$a_j^\dagger |n_1, n_2, \ldots n_j, \ldots\rangle = (-1)^{S_j} (1 - n_j) |n_1, n_2, \ldots n_j + 1, \ldots\rangle. \tag{2.2}$$

They obey the anticommutation rules

$$[a_i, a_j]_+ = [a_i^\dagger, a_j^\dagger]_+ = 0 \quad \text{and} \quad [a_i, a_j^\dagger]_+ = \delta_{ij}. \tag{2.3}$$

We shall require the occupation-number representation of one-body and two-body operators. A one-body operator T may be represented by

$$T = \sum_{\alpha,\beta} (\alpha|t|\beta)\, a_\alpha^\dagger a_\beta, \tag{2.4}$$

where $(\alpha|t|\beta) = \int d\vec{x}\, \psi_\alpha^\dagger(\vec{x})\, t(\vec{x})\, \psi_\beta(\vec{x})$, $t(\vec{x})$ being the coordinate representation of the operator, and $\psi_\alpha(\vec{x})$ and $\psi_\beta(\vec{x})$ single-particle wave functions. The two-body operators are of the form

$$V = \tfrac{1}{2} \sum_{\alpha,\beta,\gamma,\delta} (\alpha\beta|v|\gamma\delta)\, a_\alpha^\dagger a_\beta^\dagger a_\gamma a_\delta, \tag{2.5}$$

where $(\alpha\beta|v|\gamma\delta) = \int d\vec{x}_2 \int d\vec{x}_1\, \psi_\alpha^\dagger(\vec{x}_1)\, \psi_\beta^\dagger(\vec{x}_2)\, v(\vec{x}_1, \vec{x}_2)\, \psi_\gamma(\vec{x}_2)\, \psi_\delta(\vec{x}_1)$.

Let us consider single-particle states of the type $|n\ell jm m_t\rangle$. The quantum number m_t is a projection in isotopic spin space, and is $+\frac{1}{2}$ for protons and $-\frac{1}{2}$ for neutrons. For convenience we will sometimes use an index such as α to stand for this set of quantum numbers, that is, $|\alpha)$ will stand for

$|n_\alpha \ell_\alpha j_\alpha m_\alpha m_{t\alpha})$. Also, $|-\alpha)$ will represent $|n_\alpha \ell_\alpha j_\alpha -m_\alpha -m_{t\alpha})$. When a nucleus would consist of closed shells were it not for the absence of a nucleon $|n_\alpha \ell_\alpha j_\alpha -m_\alpha -m_{t\alpha}) = |-\alpha)$, it has the rotational properties of a particle $|\alpha)$. Therefore, a hole due to the absence of the $|-\alpha)$ particle will be labelled by $|\bar{\alpha}) = |\bar{n}_\alpha \bar{\ell}_\alpha \bar{j}_\alpha \bar{m}_\alpha \bar{m}_{t\alpha})$.

We write $|n_1 \ell_1 j_1 m_1 m_{t1}; \bar{n}_2 \bar{\ell}_2 \bar{j}_2 \bar{m}_2 \bar{m}_{t2})$ for the state in which a nucleon has been raised to the $|n_1 \ell_1 j_1 m_1 m_{t1})$ state, creating a hole of type $|\bar{n}_2 \bar{\ell}_2 \bar{j}_2 \bar{m}_2 \bar{m}_{t2})$ in an otherwise closed shell. It will be convenient to use the notation

$$|(\alpha\bar{\beta}) JM T M_T) = \sum_{m_\alpha, \bar{m}_\beta, m_{t\alpha}, \bar{m}_{t\beta}} (j_\alpha m_\alpha \bar{j}_\beta \bar{m}_\beta | JM)\left(\tfrac{1}{2} m_{t\alpha} \tfrac{1}{2} \bar{m}_{t\beta} | T M_T\right) \times |n_\alpha \ell_\alpha j_\alpha m_\alpha m_{t\alpha}; \bar{n}_\beta \bar{\ell}_\beta \bar{j}_\beta \bar{m}_\beta \bar{m}_{t\beta}). \tag{2.6}$$

We now choose a definite order of states in our occupation-number representation $|n_\alpha, n_\beta, n_\gamma \ldots\rangle$. (The order chosen will lead to the phase relationships of Bell (1959).) If the lowest energy level is the $[n_1 l_1 j_1]$ level, then we shall take $|\alpha) = |n_1\ \ell_1\ j_1\ -j_1\ -\tfrac{1}{2})$, $|\beta) = |n_1\ \ell_1\ \ j_1\ -j_1\ +\tfrac{1}{2})$, $|\gamma) = |n_1\ \ell_1\ j_1\ -j_1+1\ -\tfrac{1}{2})$, and so on working through the shells in order of their energy. We consider the ground state of a nucleus for which both proton and neutron shells are filled. In the Tamm-Dancoff approximation its occupation-number representation is of the form $|g\rangle = |1,1,1 \ldots 1,1,0,0,0 \ldots\rangle$. The states are all occupied up to the Fermi level and unoccupied above it. For the ground state, because of the ordering chosen, we get

$$a_\alpha |g\rangle = a_\alpha |\ldots, n_\alpha, \ldots\rangle = (-1)^{j_\alpha + m_\alpha + \frac{1}{2} + m_{t\alpha}} n_\alpha |\ldots, n_\alpha - 1, \ldots\rangle = (-1)^{j_\alpha + m_\alpha + \frac{1}{2} + m_{t\alpha}} n_\alpha |-\bar{\alpha}\rangle . \tag{2.7}$$

We are now in a position to calculate matrix elements of the residual interaction V, making use of occupation-number representation. The states which we wish to use to represent excited states of the unperturbed Hamiltonian are of the type $|(\alpha\bar{\beta}) JM T M_T\rangle$. In obvious notation

$$\langle(\alpha\bar{\beta})JMTM_T|V|(\gamma\bar{\delta})J'M'T'M_T'\rangle = \sum_{\substack{m's,\ m_t's \\ \bar{m}'s,\ \bar{m}_t's}} (j_\alpha m_\alpha j_\beta \bar{m}_\beta | JM)(j_\gamma m_\gamma j_\delta \bar{m}_\delta | J'M')$$

$$\times (\tfrac{1}{2} m_{t\alpha} \tfrac{1}{2} \bar{m}_{t\beta} | TM_T)(\tfrac{1}{2} m_{t\gamma} \tfrac{1}{2} \bar{m}_{t\delta} | T'M_T') \langle n_\alpha l_\alpha j_\alpha m_\alpha m_{t\alpha}; \bar{n}_\beta \bar{l}_\beta j_\beta \bar{m}_\beta \bar{m}_{t\beta} | v | n_\gamma l_\gamma j_\gamma m_\gamma m_{t\gamma}; \bar{n}_\delta \bar{l}_\delta j_\delta \bar{m}_\delta \bar{m}_{t\delta} \rangle. \tag{2.8}$$

It is assumed that V is independent of orientation of the nucleus, and that the charge of the nucleus is conserved. This means the matrix element is non-zero only for M' = M and $M_T' = M_T$. The matrices will be limited to those in which all states have a given J and T. The matrix elements involving particle and hole functions can be changed to ones involving only particle functions. Recoupling of angular momenta in the resulting expression gives

$$\langle(\alpha\bar{\beta})JMTM_T|V|(\gamma\bar{\delta})JMTM_T\rangle = -\sum_{J',T'} (2J'+1)(2T'+1) \begin{Bmatrix} j_\alpha & j_\beta & J \\ j_\gamma & j_\delta & J' \end{Bmatrix} \begin{Bmatrix} \frac{1}{2} & \frac{1}{2} & T \\ \frac{1}{2} & \frac{1}{2} & T' \end{Bmatrix}$$

$$\times \Big\{ ((\alpha\delta)J'M'T'M_T'|v|(\beta\gamma)J'M'T'M_T') - (-1)^{j_\beta + j_\gamma - J' + \frac{1}{2} + \frac{1}{2} - T'} ((\alpha\delta)J'M'T'M_T'|v|(\gamma\beta)J'M'T'M_T') \Big\}. \tag{2.9}$$

Details of these calculations appear in Appendix A.

It is assumed that the isotopic spin part of v may be factored out. Simplification of the remaining angular momentum terms may be done in either one of two ways. The first way is to carry out a multipole expansion of the potential and use Slater integrals to evaluate the matrix elements (equations 27 and 30 of Lewis and Walecka (1964)). The second method is to change to LS coupling and (i) carry out the multipole expansion and use Slater integrals (Gillet (1962)), or (ii) if the single-particle wave functions are simple harmonic oscillator wave functions, use the transformation brackets (tabulated by Brody and Moshinsky (1960))* to separate center-of-mass and relative coordinates for two particles. (See equation 40 of Lewis and Walecka (1964).)

If the residual interaction is of finite range with Gaussian or Yukawa

*Brody, T.A. and Moshinsky, M. 1960. Tables of Transformation Brackets (Universidad Nacional Autonoma de Mexico).

radial dependence, say, the Slater integrals become very complicated and the easiest way to evaluate matrix elements probably is to use transformation brackets. For a zero-range type of residual interaction the Slater integrals are reasonably easy to compute. This is fortunate, since the method of transformation brackets cannot be applied to a zero-range potential.

One is now in a position to calculate matrix elements of the Hamiltonian $H_o + V$. The eigenstates found by diagonalizing the matrix can be applied to calculation of inelastic electron scattering cross sections.

Chapter 3

INELASTIC ELECTRON SCATTERING CROSS SECTIONS

A very good discussion of inelastic scattering cross sections is given by Willey (1963). This section will be essentially a summary of the results given in his paper, modified for the simple particle-hole model where necessary. Another difference between Willey's development and this one is in the definition of the multipole operators. Willey's operators contain a factor $(2\lambda + 1)!!/q^{\lambda}$ so that his nuclear matrix elements might be compared with earlier work in which matrix elements contained r^{λ} instead of $j_{\lambda}(qr)$. (For $qr \ll 1$, $j_{\lambda}(qr) \simeq (qr)^{\lambda}/(2\lambda + 1)!!$.) Since the coefficients of the squares of his nuclear matrix elements contain a factor $q^{2\lambda}[(2\lambda + 1)!!]^{-2}$, this factor drops out of the final result. His electric and magnetic multipole operators contain a factor $[\lambda/\lambda+1]^{\frac{1}{2}}$ which disappears in a similar manner. These factors shall be ignored here, so that our multipole operators are the same as those given in equation 3 of Lewis and Walecka (1964).

A cross section is obtained by dividing the rate of transition to the state of interest (the dW/dt of Chapter 1) by the incident flux of electrons. To find the transition rate we shall have to determine the interaction matrix element $\langle F|H'|I\rangle$. The interaction is, of course, the electromagnetic interaction of the electron with the charge, current, and magnetic moment of the nucleus.

The field produced by an electron is expressed in terms of spherical harmonic functions (a multipole expansion). The result is that the cross section may be expressed as

$$\frac{d\sigma}{d\Omega} = \sum_{\lambda=0}^{\infty} \frac{d\sigma_{C\lambda}}{d\Omega} + \sum_{\lambda=1}^{\infty} \frac{d\sigma_{E\lambda}}{d\Omega} + \sum_{\lambda=1}^{\infty} \frac{d\sigma_{M\lambda}}{d\Omega} . \qquad (3.1)$$

The subscript C refers to the longitudinal terms in the expansion of the field. E and M refer to electric and magnetic terms in the transverse part

of the field, which corresponds to the field of real photons (Preston (1962), Chapter 11). The excitation of the nucleus may be attributed to the absorption of a virtual photon of a particular angular momentum and parity. We find that we need consider only a few terms in the multipole expansion of the cross section. For instance, the cross section for excitation from the ground state of C^{12} ($J=0$, $\pi=+1$) to the giant dipole resonance ($J=1$, $\pi=-1$) can be calculated using only the terms $\frac{d\sigma_{C1}}{d\Omega}$ and $\frac{d\sigma_{E1}}{d\Omega}$. All other terms are forbidden by parity or angular momentum selection rules.

Willey gives general results for the multipole cross sections (equations 2.24, Willey (1963)).

$$\frac{d\sigma_{C\lambda}}{d\Omega} = 16\pi\left(\frac{e^2}{\hbar c}\right)^2\left(\frac{k_f}{k_i}\right)^2 \frac{\cos^2\left(\frac{\theta}{2}\right)}{k_i^2\left[1+(k_f/k_i)^2-2(k_f/k_i)\cos\theta\right]^2} \frac{1}{2J_i+1}\left|(f\|M(C\lambda)\|i)\right|^2$$

$$= 16\pi\left(\frac{e^2}{\hbar c}\right)^2 \frac{k_f^2}{q^4}\cos^2\left(\frac{\theta}{2}\right)\frac{1}{2J_i+1}\left|(f\|M(C\lambda)\|i)\right|^2. \qquad (3.2)$$

θ is the electron scattering angle in the laboratory system, k_i and k_f the wave-numbers of the incident and scattered electron, $\hbar q$ the three-momentum transfer, $|i)$ and $|f)$ the initial and final states of the nucleus. The coulomb multipole operator is

$$M(C\lambda,\mu) = \int j_\lambda(qr)\, Y_\lambda^\mu(\hat{r})\,\rho_N(\vec{r})\,d\vec{r}. \qquad (3.3)$$

We shall be considering closed shell nuclei with $M_T = 0$ for initial and final states, so the matrix element $\left|(f\|M(C\lambda)\|i)\right|^2$ is not reduced with respect to isotopic spin.

For the electric multipoles we have

$$\frac{d\sigma_{E\lambda}}{d\Omega} = \left(\frac{k_f}{k_i}\right)^2\left(\frac{e^2}{\hbar c}\right)^2 \frac{4\pi}{k_i^2} \frac{k_i^2+k_f^2+k_ik_f(1-\cos\theta)}{2k_f^2(1-\cos\theta)\left[1+(k_f/k_i)^2-2(k_f/k_i)\cos\theta\right]} \frac{1}{2J_i+1}\left|(f\|M(E\lambda)\|i)\right|^2$$

$$\frac{d\sigma_{E\lambda}}{d\Omega} = \pi\left(\frac{e^2}{\hbar c}\right)^2 \frac{1}{q^2 \sin(\theta/2)}\left[1 + \left(\frac{k_f}{k_i}\right)^2 + 2\left(\frac{k_f}{k_i}\right)\sin^2\left(\frac{\theta}{2}\right)\right] \frac{1}{2J_i+1}$$

$$\times \left|(f\|M(E\lambda)\|i)\right|^2. \tag{3.4}$$

$$M(E\lambda,\mu) = \frac{1}{q}\int\left\{\frac{1}{c}\vec{j}_N \cdot \vec{\nabla} \times j_\lambda(qr)\vec{\mathcal{Y}}^{\mu}_{\lambda\lambda}(\hat{r}) + q^2 j_\lambda(qr)\vec{\mathcal{Y}}^{\mu}_{\lambda\lambda}\cdot\vec{\mu}_N(\vec{r})\right\}d\vec{r}, \tag{3.5}$$

where $\vec{\mathcal{Y}}^{\mu}_{\lambda\lambda}(\hat{r})$ is a vector spherical harmonic (Edmonds (1960), section 5.9) and $\vec{j}_N$ and $\vec{\mu}_N$ are the nuclear current and magnetization density operators.

The result for magnetic multipoles is

$$\frac{d\sigma_{M\lambda}}{d\Omega} = \pi\left(\frac{e^2}{\hbar c}\right)^2 \frac{1}{q^2 \sin^2(\theta/2)}\left[1 + \left(\frac{k_f}{k_i}\right)^2 + 2\left(\frac{k_f}{k_i}\right)\sin^2\left(\frac{\theta}{2}\right)\right] \frac{1}{2J_i+1}$$

$$\times \left|(f\|M(M\lambda)\|i)\right|^2 \tag{3.6}$$

with

$$M(M\lambda,\mu) = \int\left\{\vec{\mu}_N(\vec{r})\cdot\vec{\nabla}\times j_\lambda(qr)\vec{\mathcal{Y}}^{\mu}_{\lambda\lambda}(\hat{r}) + j_\lambda(qr)\vec{\mathcal{Y}}^{\mu}_{\lambda\lambda}(\hat{r})\cdot\vec{j}_N(\vec{r})\right\}d\vec{r}. \tag{3.7}$$

We shall consider simplicifation of these results for the case when $|i)$ and $|f)$ are states given by the simple (Tamm-Dancoff) particle-hole model for closed-shell nuclei. The initial state is the unperturbed ground state $|g)$. The final state is a linear combination of particle-hole eigenstates of H_o, say

$$|f) = \sum_{\alpha\bar{\beta}} C_{\alpha\bar{\beta}} |(\alpha\bar{\beta})JMTM_T). \tag{3.8}$$

Then, if X_λ represents one of the multipole operators, we have

$$(f'\|X_\lambda\|i) = (J_{f'}0\,T0|X^\circ_\lambda|g)\frac{1}{(-1)^{J_{f'}}\begin{pmatrix} J_{f'} & \lambda & 0\\ 0 & 0 & 0\end{pmatrix}} = \sqrt{2\lambda+1}\,(\lambda 0\,T0|X^\circ_\lambda|g)$$

by equations 5.4.1 and 3.7.9 of Edmonds (1960). This means that

$$(f\|X_\lambda\|i) = \sqrt{2\lambda+1}\sum_{\alpha\bar{\beta}} C^*_{\alpha\bar{\beta}}\,((\alpha\bar{\beta})\lambda 0\,T0|X^\circ_\lambda|g).$$

The operators are of a form such that their isotopic spin dependence may be factored out, that is, $X^0_\lambda = N^0_\lambda [\frac{1}{2}(\eta_0 + \eta_1 \tau_3)]$, where N^0_λ operates on space and spin coordinates only. It is shown in Appendix B that

$$\sqrt{2\lambda+1}\,((\alpha\bar{\beta})\lambda 0\, T0 | X^0_\lambda | g) = \frac{-1}{\sqrt{2}}(\alpha \| N_\lambda \eta_T \| \beta),$$

where $|\alpha)$ and $|\beta)$ are single-particle wave functions. Hence we have

$$((\alpha\bar{\beta})\lambda T0 \| X_\lambda \| g) = \frac{-n_T}{\sqrt{2}} \sum_{\alpha\beta} C^*_{\alpha\bar{\beta}}\,(\alpha \| N_\lambda \| \beta). \tag{3.9}$$

For single-particle shell model functions the density operators give

$$(\psi_f(\vec{y}) | \rho_N(\vec{r}) | \psi_i(\vec{y})) = \left[\varepsilon_T + \frac{1}{8}\frac{\hbar^2 q^2}{M^2 c^2}(\varepsilon_T - 2\gamma_T)\right] \int d\vec{y}\, \delta(\vec{r}-\vec{y})\, \psi_f^\dagger(\vec{y})\, \psi_i(\vec{y}) \tag{3.10}$$

$$(\psi_f(\vec{y}) | \vec{j}_N(\vec{r}) | \psi_i(\vec{y})) = \frac{\varepsilon_T}{2M} \int d\vec{y}\, \delta(\vec{r}-\vec{y}) \left\{ \psi_f^\dagger(\vec{y})\, \vec{p}(\vec{y})\, \psi_i(\vec{y}) + [\vec{p}(\vec{y})\, \psi_f(\vec{y})]^\dagger \psi_i(\vec{y}) \right\} \tag{3.11}$$

$$(\psi_f(\vec{y}) | \vec{\mu}_N(\vec{r}) | \psi_i(\vec{y})) = \frac{\hbar \gamma_T}{2Mc} \int d\vec{y}\, \delta(\vec{r}-\vec{y})\, \psi_f^\dagger(\vec{y})\, \vec{\sigma}\, \psi_i(\vec{y}) \tag{3.12}$$

(cf. equations 2.57, 2.58, and 2.59 of Willey (1963)). The values of the ε_T are:

$$\varepsilon_0 = \varepsilon_p + \varepsilon_n = 1 \qquad \gamma_0 = \gamma_p + \gamma_n = 0.88$$

$$\varepsilon_1 = \varepsilon_p - \varepsilon_n = 1 \qquad \gamma_1 = \gamma_p - \gamma_n = 4.70\ .$$

We are now in a position to calculate the three types of matrix elements. The simplest is the coulomb type,

$$((\alpha\bar{\beta})\lambda T0 \| M(C\lambda) \| g) = \frac{-1}{\sqrt{2}}\left[\varepsilon_T + \frac{1}{8}\frac{\hbar^2 q^2}{M^2 c^2}(\varepsilon_T - 2\gamma_T)\right](\alpha \| j_\lambda(qr) Y_\lambda(\hat{r}) \| \beta).$$

This may be reduced using expressions 7.1.7 and 5.4.5 in Edmonds (1960). One obtains

$$\left((\alpha\bar{\beta})\lambda T0\|M(C\lambda)\|g\right) = -\left[\varepsilon_T + \frac{1}{8}\frac{\hbar^2 q^2}{M^2c^2}(\varepsilon_T - 2\gamma_T)\right]\sqrt{\frac{(2l_\alpha+1)(2l_\beta+1)(2\lambda+1)}{8\pi}}$$

$$\times\sqrt{(2j_\beta+1)(2j_\alpha+1)}\,(-1)^{j_\beta+\frac{1}{2}+\lambda}\begin{Bmatrix} l_\alpha & l_\beta & \lambda \\ j_\beta & j_\alpha & \frac{1}{2}\end{Bmatrix}\begin{pmatrix} l_\alpha & l_\beta & \lambda \\ 0 & 0 & 0\end{pmatrix}\int_0^\infty r^2 dr\, R_\alpha R_\beta j_\lambda(qr)$$

$$= \left[\varepsilon_T + \frac{1}{8}\left(\frac{\hbar q}{Mc}\right)^2(\varepsilon_T - 2\gamma_T)\right]\sqrt{\frac{(2j_\alpha+1)(2j_\beta+1)(2\lambda+1)}{8\pi}}\,(-1)^{j_\alpha+\frac{1}{2}}$$

$$\times\begin{pmatrix} j_\alpha & \lambda & j_\beta \\ \frac{1}{2} & 0 & -\frac{1}{2}\end{pmatrix}\left[\frac{1+(-1)^{l_\alpha+l_\beta+\lambda}}{2}\right]\int_0^\infty r^2 dr\, R_\alpha R_\beta j_\lambda(qr), \qquad (3.13)$$

where R_α and R_β are the radial parts of single-particle wave functions.

To reduce the electric multipole matrix elements, we make use of a property of the vector spherical harmonics (Willey (1963), equations 2.37 and 2.51) and of the continuity equation to change

$$\vec{j}_N\cdot\vec{\nabla}\times j_\lambda(qr)\,\vec{\mathcal{Y}}^\mu_{\lambda\lambda}(\hat{r})$$

to

$$\frac{-i}{\sqrt{\lambda(\lambda+1)}}\left\{(1+\vec{r}\cdot\vec{\nabla})j_\lambda(qr)\,Y^\mu_\lambda(\hat{r})\,\vec{\nabla}\cdot\vec{j}_N - q^2 j_\lambda(qr)\,Y^\mu_\lambda(\hat{r})\,\vec{r}\cdot\vec{j}_N\right\}$$

$$= \frac{-1}{\hbar\sqrt{\lambda(\lambda+1)}}\left\{[H,\rho_N]\left(1+r\frac{\partial}{\partial r}\right)j_\lambda(qr)\,Y^\mu_\lambda(\hat{r}) - iq^2 j_\lambda(qr)\,Y^\mu_\lambda(\hat{r})\,\vec{r}\cdot\vec{j}_N\right\}.$$

Hence we get

$$\left((\alpha\bar{\beta})\lambda T0\|M(E\lambda)\|g\right) = \frac{-1}{\sqrt{2}}\left(\alpha\left\|\int\left\{\left[-\frac{E_\beta - E_\alpha}{\hbar q}\rho_N\left(1+r\frac{\partial}{\partial r}\right)j_\lambda(qr)\,Y_\lambda(\hat{r})\right.\right.\right.$$

$$\left.\left.\left. + iq\,j_\lambda(qr)\,Y_\lambda(\hat{r})\,\vec{r}\cdot\vec{j}_N\right]\frac{1}{c\sqrt{\lambda(\lambda+1)}} + q\,j_\lambda(qr)\,\vec{\mathcal{Y}}_{\lambda\lambda}\cdot\vec{\mu}_N\right\}d\vec{r}\,\right\|\beta\right)$$

$$= \frac{-1}{\sqrt{2}}\left\{\varepsilon_T\frac{1}{\sqrt{\lambda(\lambda+1)}}(l_\alpha j_\alpha\|Y_\lambda\|l_\beta j_\beta)\int_0^\infty r^2\left[-\frac{E_\alpha - E_\beta}{\hbar cq}\left(1+r\frac{\partial}{\partial r}\right)j_\lambda R_\alpha R_\beta\right.\right.$$

$$\left.\left. + \frac{\hbar q}{2Mc}j_\lambda\left(rR_\alpha\frac{dR_\beta}{dr} - rR_\beta\frac{dR_\alpha}{dr}\right)\right]dr + \frac{\hbar q\gamma_T}{2Mc}(l_\alpha j_\alpha\|\vec{\mathcal{Y}}_{\lambda\lambda}\cdot\vec{\sigma}\|l_\beta j_\beta)\int_0^\infty r^2 j_\lambda R_\alpha R_\beta\,dr\right\}$$

$$= -\sqrt{\frac{(2l_\alpha+1)(2l_\beta+1)(2j_\alpha+1)(2j_\beta+1)(2\lambda+1)}{8\pi}} \begin{pmatrix} l_\alpha & l_\beta & \lambda \\ 0 & 0 & 0 \end{pmatrix} \left[\left\{ \frac{E_\alpha - E_\beta}{\hbar c q} \int_0^\infty r^2 j_\lambda(qr) \right.\right.$$

$$\times \left[r R_\beta \frac{dR_\alpha}{dr} + r R_\alpha \frac{dR_\beta}{dr} + 2 R_\alpha R_\beta \right] dr + \frac{\hbar q}{2Mc} \int_0^\infty r^2 j_\lambda(qr) \left[r R_\alpha \frac{dR_\beta}{dr} \right.$$

$$\left.\left. - r R_\beta \frac{dR_\alpha}{dr} \right] dr \right\} \frac{\varepsilon_T (-1)^{j_\beta + \frac{1}{2} + \lambda}}{\sqrt{\lambda(\lambda+1)}} \begin{Bmatrix} l_\alpha & l_\beta & \lambda \\ j_\beta & j_\alpha & \frac{1}{2} \end{Bmatrix} + \frac{\hbar q}{Mc} \gamma_T \sqrt{\frac{3(2\lambda+1)}{2}} (-1)^{l_\alpha}$$

$$\times \begin{Bmatrix} l_\alpha & l_\beta & \lambda \\ \frac{1}{2} & \frac{1}{2} & 1 \\ j_\alpha & j_\beta & \lambda \end{Bmatrix} \left. \int_0^\infty r^2 j_\lambda(qr) R_\alpha R_\beta \, dr \right]$$

$$= -\sqrt{\frac{(2\lambda+1)(2j_\alpha+1)(2j_\beta+1)}{8\pi}} \left[\frac{\varepsilon_T (-1)^{j_\beta + \lambda - \frac{1}{2}}}{\sqrt{\lambda(\lambda+1)}} \begin{pmatrix} j_\alpha & j_\beta & \lambda \\ \frac{1}{2} & -\frac{1}{2} & 0 \end{pmatrix} \left\{ \frac{E_\alpha - E_\beta}{\hbar c q} \int_0^\infty r^2 j_\lambda(qr) \right.\right.$$

$$\times \left(r R_\alpha R'_\beta + r R'_\alpha R_\beta + 2 R_\alpha R_\beta \right) dr + \frac{\hbar q}{2Mc} \int_0^\infty r^2 j_\lambda(qr) \left(r R'_\beta R_\alpha - r R_\beta R'_\alpha \right) dr \left.\right\}$$

$$+ \frac{\hbar q}{Mc} \gamma_T \sqrt{\frac{3(2\lambda+1)(2l_\alpha+1)(2l_\beta+1)}{2}} (-1)^{l_\alpha} \begin{Bmatrix} l_\alpha & l_\beta & \lambda \\ \frac{1}{2} & \frac{1}{2} & 1 \\ j_\alpha & j_\beta & \lambda \end{Bmatrix} \begin{pmatrix} l_\alpha & l_\beta & \lambda \\ 0 & 0 & 0 \end{pmatrix}$$

$$\times \int_0^\infty r^2 j_\lambda R_\alpha R_\beta \, dr \quad . \tag{3.14}$$

This may be compared with equation 3.5 of Jolly (1964). Equation 3.11 of the Jolly report is written with a term $-2R_\alpha R_\beta$, which is incorrect.

If the radial wave functions are harmonic oscillator functions and if $E_\alpha - E_\beta = 1\hbar\omega$, then we have $\frac{E_\alpha - E_\beta}{\hbar} = \omega = \frac{\hbar}{Mb^2}$.

Hence, where $\lambda\!\!\!^{-}_M = \frac{\hbar}{Mc} = 0.21 \text{ fm}$ is the reduced Compton wavelength of a nucleon,

$$((\alpha\bar{\beta})\lambda T0\|M(E\lambda)\|q) = -\frac{\lambda_M}{b}\sqrt{\frac{(2\lambda+1)(2j_\alpha+1)(2j_\alpha+1)}{8\pi}}\left[\frac{\varepsilon_T(-1)^{j_\beta-\frac{1}{2}+\lambda}}{\sqrt{\lambda(\lambda+1)}}\begin{pmatrix} j_\alpha & j_\beta & \lambda \\ \frac{1}{2} & -\frac{1}{2} & 0\end{pmatrix}\right.$$

$$\times\left\{\frac{1}{qb}\int_0^\infty r^2 j_\lambda(qr)\left(R_\alpha R'_\beta r + r R'_\alpha R_\beta + 2R_\alpha R_\beta\right)dr + \frac{qb}{2}\int_0^\infty r^2 j_\lambda(qr)\right.$$

$$\left.\times\left(rR'_\beta R_\alpha - rR_\beta R'_\alpha\right)dr\right\} + (qb)\gamma_T\sqrt{\frac{3(2\lambda+1)(2l_\alpha+1)(2l_\beta+1)}{2}}(-1)^{l_\alpha}$$

$$\left.\times\begin{Bmatrix} l_\alpha & l_\beta & \lambda \\ \frac{1}{2} & \frac{1}{2} & 1 \\ j_\alpha & j_\beta & \lambda\end{Bmatrix}\begin{pmatrix} l_\alpha & l_\beta & \lambda \\ 0 & 0 & 0\end{pmatrix}\int_0^\infty r^2 j_\lambda(qr) R_\alpha R_\beta\, dr\right]. \qquad (3.15)$$

For the magnetic multipoles we get (cf. equation 2.64c of Willey (1964))

$$((\alpha\bar{\beta})\lambda T0\|M(M\lambda)\|q) = \frac{-\lambda_M q}{\sqrt{2}}\left\{\frac{\varepsilon_T}{\sqrt{\lambda(\lambda+1)}}(R_\alpha|j_{\lambda+1}|R_\beta)(l_\alpha j_\alpha\|\vec{Y}_{\lambda\lambda+1}\cdot\vec{l}\|l_\beta j_\beta)\right.$$

$$+\frac{\varepsilon_T}{\sqrt{(\lambda+1)(2\lambda+1)}}(R_\alpha|j_{\lambda-1}|R_\beta)(l_\alpha j_\alpha\|\vec{Y}_{\lambda\lambda-1}\cdot\vec{l}\|l_\beta j_\beta) - \frac{1}{2}\gamma_T\sqrt{\frac{\lambda}{2\lambda+1}}$$

$$\left.\times(R_\alpha|j_{\lambda+1}|R_\beta)(l_\alpha j_\alpha\|\vec{Y}_{\lambda\lambda+1}\cdot\vec{\sigma}\|l_\beta j_\beta) + \frac{1}{2}\gamma_T\sqrt{\frac{\lambda+1}{2\lambda+1}}(R_\alpha|j_{\lambda-1}|R_\beta)(l_\alpha j_\alpha\|\vec{Y}_{\lambda\lambda-1}\cdot\vec{\sigma}\|l_\beta j_\beta)\right\}$$

$$= -\lambda_M q\sqrt{\frac{(2l_\alpha+1)(2l_\beta+1)(2j_\alpha+1)(2j_\beta+1)}{8\pi}}\left\{\varepsilon_T(-1)^{j_\beta-\frac{1}{2}+\lambda}\begin{Bmatrix} l_\alpha & j_\alpha & \frac{1}{2} \\ j_\beta & l_\beta & \lambda\end{Bmatrix}\delta_{l_\alpha l_\beta}\right.$$

$$\times\sqrt{l_\beta(l_\beta+1)(2l_\beta+1)}\left[\sqrt{\frac{2\lambda+3}{\lambda}}\begin{Bmatrix} \lambda+1 & 1 & \lambda \\ l_\beta & l_\alpha & l_\beta\end{Bmatrix}\begin{pmatrix} l_\alpha & \lambda+1 & l_\beta \\ 0 & 0 & 0\end{pmatrix}\int_0^\infty r^2 j_{\lambda+1}(qr) R_\alpha R_\beta\, dr\right.$$

$$\left.+\sqrt{\frac{2\lambda-1}{\lambda+1}}\begin{Bmatrix} \lambda-1 & 1 & \lambda \\ l_\beta & l_\alpha & l_\beta\end{Bmatrix}\begin{pmatrix} l_\alpha & \lambda-1 & l_\beta \\ 0 & 0 & 0\end{pmatrix}\int_0^\infty r^2 j_{\lambda-1} R_\alpha R_\beta\, dr\right]$$

$$+(-1)^{l_\alpha}\gamma_T\sqrt{\frac{3}{2}}\left[\sqrt{(2\lambda-1)(\lambda+1)}\begin{Bmatrix} l_\alpha & l_\beta & \lambda-1 \\ \frac{1}{2} & \frac{1}{2} & 1 \\ j_\alpha & j_\beta & \lambda\end{Bmatrix}\begin{pmatrix} l_\alpha & \lambda-1 & l_\beta \\ 0 & 0 & 0\end{pmatrix}\int_0^\infty r^2 j_{\lambda-1}(qr) R_\alpha R_\beta dr\right.$$

$$-\sqrt{\lambda(2\lambda+3)}\begin{Bmatrix} \ell_\alpha & \ell_\beta & \lambda+1 \\ \frac{1}{2} & \frac{1}{2} & 1 \\ j_\alpha & j_\beta & \lambda \end{Bmatrix}\begin{pmatrix} \ell_\alpha & \lambda+1 & \ell_\beta \\ 0 & 0 & 0 \end{pmatrix}\int_0^\infty r^2 j_{\lambda+1}(qr) R_\alpha R_\beta \, dr \Bigg]\Bigg\}. \qquad (3.16)$$

If the radial wave functions are harmonic oscillator functions, some of the radial integrals may be found in Tassie (1957). Integrals not given in Tassie's table may be calculated using equation 50 of Lewis and Walecka (1964). One source of values of 9-j symbols is Matsunobu and Takebe (1955).

Particle-hole model calculations of cross sections for inelastic electron scattering can be made by taking the appropriate combination of equations 3.1, 3.2, 3.4, 3.6, 3.9, 3.13, 3.14, and 3.16.

Willey also gives two correction terms which should be included in the matrix elements (Willey (1963), equations 2.67, 2.68). One term corrects for center-of-mass motion which can arise when a fixed oscillator potential is used; the other corrects for the finite size of nucleons. The center-of-mass motion correction can be made by multiplying the matrix element by a factor $\exp(q^2b^2/4A)$, where A is the mass number of the target nucleus. A similar factor $\exp(-q^2a_p^2/4)$, where $a_p^2 = 0.43$ fm^2, allows for the finite size of nucleons. The effect of these two corrections is to change a factor $\exp(-q^2b^2/2)$ to $\exp[-\frac{1}{2}q^2(\frac{A-1}{A}b^2 + a_p^2)]$ in expressions for the cross section.

Chapter 4

MEASUREMENT OF INELASTIC SCATTERING CROSS SECTIONS

§1 Electron Scattering Facilities at the Saskatchewan Accelerator Laboratory

The electron linear accelerator at Saskatchewan is an S-band travelling wave machine. The electron beam is pulsed; pulse widths may be varied from 10 nanoseconds to 1 microsecond, and the repetition rate from single shot to 1400 pulses per second. The energy distribution of the output electron beam is approximately Gaussian, with a full-width-at-half-maximum of approximately 3%. The maximum peak current available from the four-section accelerator is related to the energy by the expression (Beer (1964))

$$i_{peak}(mA) = 4.9[141 - E(MeV)]. \qquad (4.1)$$

At present, for most energies, the upper limit to current is set, not by the accelerator load line, but by the amount of power that the beam transport system is capable of dissipating.

The output beam will be directed towards the electron scattering area by two 45^{o} bending magnets. (See figure 4.1.) The momentum defining slits, between the bending magnets, transmit only those electrons within a preselected momentum range. The magnetic components of the transport system are designed to have a momentum resolution of 1 part in 2000. The beam is focussed by magnetic quadrupole pairs.

Thin targets will be located at the center of a cylindrical aluminum scattering chamber 25 inches in diameter. The beam transmitted through the target passes out of the chamber into a Faraday cup or beam catcher. Electrons scattered from the target will be momentum-analyzed by means of a double-focussing 180^{o} magnetic spectrometer. The spectrometer vacuum chamber will be coupled directly to one of a number of scattering chamber ports. The ports permit the spectrometer to be set at scattering angles

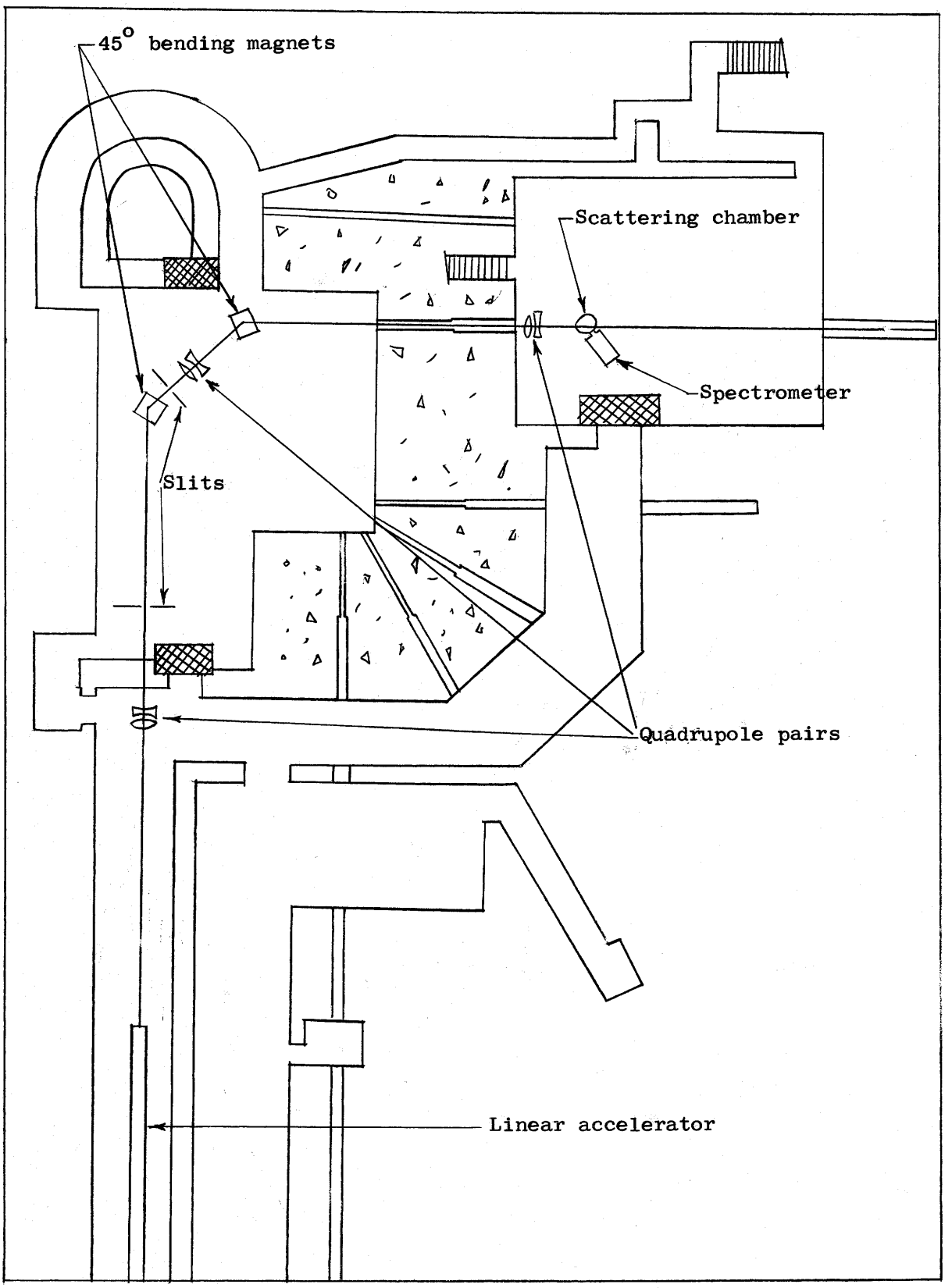

Fig. 4.1 Electron scattering system at the Saskatchewan Accelerator Laboratory.

of 30^{o}, 45^{o}, 60^{o}, 75^{o}, 90^{o}, 110^{o}, 125^{o}, 140^{o}, and 155^{o}. The solid angle of acceptance of the spectrometer is about 5 millisteradians. Acceptance angle is approximately 2.5^{o} in the plane of scattering and 6.5^{o} perpendicular to the scattering plane for electrons scattered from the center of the chamber. Electrons analyzed by the spectrometer will be detected by a scintillation counter and Cerenkov counter in coincidence. At the optic axis, for a source 19.6 inches from the spectrometer pole face, the dispersion is 5×10^{-4} per millimeter in the waist plane (Sykes (1965)).

The primary measurement of the number of electrons incident upon the target will be made by the collection of the beam in a Faraday cup placed behind the scattering chamber. Should the Faraday cup give rise to a large background at the electron detection system, it will be necessary to use a calibrated secondary emission monitor to measure beam current.

§2 Experimental Procedure

A general procedure for measuring inelastic scattering cross sections has evolved at existing electron accelerator establishments such as the ones at Stanford, Orsay, and Darmstadt. Undoubtedly this procedure will be followed for the first inelastic scattering work at the Saskatchewan Accelerator Laboratory.

Electrons incident upon the target have their energies within a band which is typically a few tenths of one per cent of the average value, E_i. The analyzing spectrometer accepts electrons from the target at an average angle θ. The target is thin, so almost all the beam passes through it; beam intensity is measured after the beam has left the scattering chamber. The magnetic field of the spectrometer is set so that scattered electrons with energies between E_f and $E_f + \Delta E_f$ reach the detection system.

Scattered electrons are counted under these conditions either for a certain period of time or until a certain number of counts have been registered. The magnetic field of the spectrometer is changed so that electrons of a different energy are counted. Counting rates are measured for a range of spectrometer settings, so that an energy spectrum of the scattered electrons is obtained for a particular incident energy and scattering angle. The energy of the incident electrons is then changed and a new spectrum obtained. When measurements have been made at the desired values of E_i, either the scattering angle or the target can be changed. To change spectrometer angle it will be necessary to uncouple the spectrometer from the scattering chamber. Consequently, for small, solid targets it will be easier to change targets than to change spectrometer angle.

The counting rate can be converted to an inelastic scattering cross section. The equation is

$$\dot{n}_e = \frac{d^2\sigma}{d\Omega dE_f} \cdot \Delta E_f \cdot \Delta\Omega \cdot N_t \frac{i}{|e|} , \qquad (4.2)$$

where

$\dot{n}_e$ is the average rate at which scattered electrons reach a detector,

$\frac{d^2\sigma}{d\Omega dE_f}$ is a double differential scattering cross section,

ΔE_f is the range of energies for which electrons may reach the detector through the spectrometer,

$\Delta\Omega$ is the solid angle of acceptance of the spectrometer,

N_t is the number of target nuclei per unit area,

i is the average current of electrons incident upon a target, and

e is the charge of an electron.

It is desirable to make the thickness of target traversed the same for all electrons scattered through an angle θ, regardless of the depth within the

target at which they were scattered. This may be done by setting the target at an angle such that the normal to the plane of the target bisects the scattering angle θ.

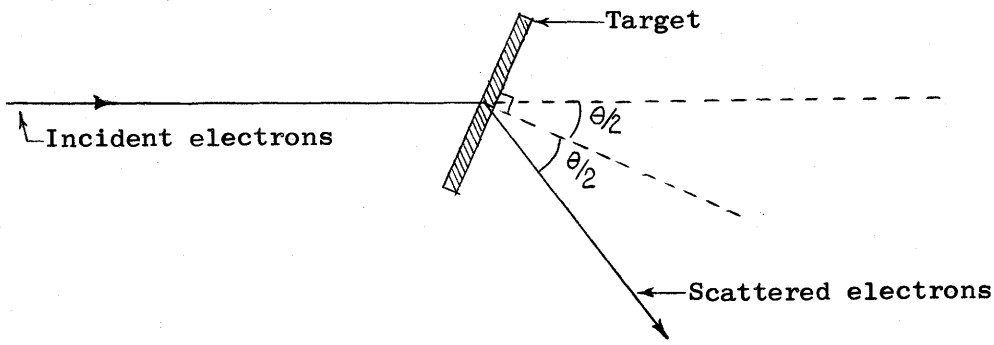

Fig. 4.2 Orientation of target with respect to the incident and scattered electrons.

When the target is set as shown in figure 4.2, N_t is given by

$$N_t = \frac{N_o \rho}{A} \cdot t \cdot \sec\left(\frac{\theta}{2}\right)$$

where N_o is Avogadro's number and ρ, A, and t the density, atomic weight, and thickness of the target.

Peaks will show up in a plot of $\frac{d^2\sigma}{d\Omega dE_f}$ vs. E_f. The area under such a peak is the differential cross section, $d\sigma/d\Omega$ (equation 3.1).

Chapter 5

CORRECTIONS TO INELASTIC SCATTERING SPECTRA

We shall be interested in measuring cross sections for inelastic electron scattering in which the target nucleus is excited to a dipole state. It will be necessary to subtract background due to other processes; these may be classified according to whether the electrons lose energy by nuclear excitation or by radiation or ionization in the target-scattering chamber system. The most important of the nuclear processes will be quasi-elastic scattering from nucleons; of the other types, the radiation tail of the elastic peak will be the most important contribution to background.

§1 Energy Losses Due to Processes Other Than Excitation of the Nucleus

It will be convenient to label the various processes which contribute to this background.

Type I background: An electron radiates a photon when undergoing elastic scattering from a nucleus; it is scattered into the solid angle of acceptance of the spectrometer, its energy reduced to E_f as a result of the radiation. The Bethe-Heitler differential cross section gives the probability for scattering of an electron with initial energy E_i into a solid angle $d\Omega_e$ and final energy E_f, with the emission of a photon of energy k into the solid angle $d\Omega_\rho$ (Heitler (1954), page 244). The photon is not detected, so the Bethe-Heitler cross section must be integrated over photon angles to give $\left(\frac{d^2\sigma}{d\Omega\, dE_f}\right)_I$, the background contribution due to bremsstrahlung produced at the target nucleus. When the nuclear form factor is included in the Bethe-Heitler cross section (see Maximon and Isabelle (1964), for example), the integration becomes too difficult to be done analytically.

Schiff (1952) obtained an approximate expression for the cross section

which we require. He made use of the fact that the photon distribution is sharply peaked in the directions of the incident or the scattered electron. He assumed that the photon is emitted in the direction either of $\vec{k}_i$ or of $\vec{k}_f$ and kept only dominant terms, which are of order $\ln(E_i/mc^2)$, where mc^2 is the rest energy of an electron. His result may be modified by including elastic form factors for the nucleus. The form factors are given by

$$|F(q)|^2 = \frac{\left(\frac{d\sigma}{d\Omega}\right)_{elastic}}{\left(\frac{d\sigma}{d\Omega}\right)_{Mott}} = \frac{\left(\frac{d\sigma}{d\Omega}\right)_{elastic}}{\left(\frac{Ze^2}{2E_i}\right)^2 \frac{\cos^2(\theta/2)}{\sin^4(\theta/2)}} \qquad (5.1)$$

Figure 5.1 gives the Mott cross section as a function of E_i for a number of values of θ. The modified result of Schiff is

$$\left(\frac{d^2\sigma}{d\Omega\, dE_f}\right)_{Schiff} = \frac{1}{137\pi}\left[\ln\left(\frac{2E_i}{mc^2}\sin\frac{\theta}{2}\right) - \frac{1}{2}\right]\left(1 + \frac{E_f^2}{E_i^2}\right)$$

$$\times \left(F^2(q_i) + \frac{E_i^2}{E_f^2}F^2(q_f)\right)\frac{1}{E_i - E_f}\left(\frac{d\sigma}{d\Omega}\right)_{Mott} \qquad (5.2)$$

where $F^2(q_i)$ and $F^2(q_f)$ are the form factors for elastic scattering at energies E_i and E_f.

Maximon and Isabelle have integrated the Bethe-Heitler cross section, keeping terms of relative order 1 as well as those of order $\ln(E_i/mc^2)$. They plot the ratio of their result to Schiff's expression for a number of values of scattering angle and of final energy at incident energies of 100 MeV and 200 MeV. For photon energies from 1% to 70% of E_i and scattering angles less than 150°, this ratio is between 0.6 and 1.0. For scattering angles greater than 150° the ratio quickly becomes greater than 1.0.

The shape and relative importance of the Schiff expression may be seen from Figure 5.2, in which the ratio $\left(\frac{d^2\sigma}{d\Omega\, dE_f}\right)_{Schiff} \Big/ \left(\frac{d\sigma}{d\Omega}\right)_{elastic}$ is plotted

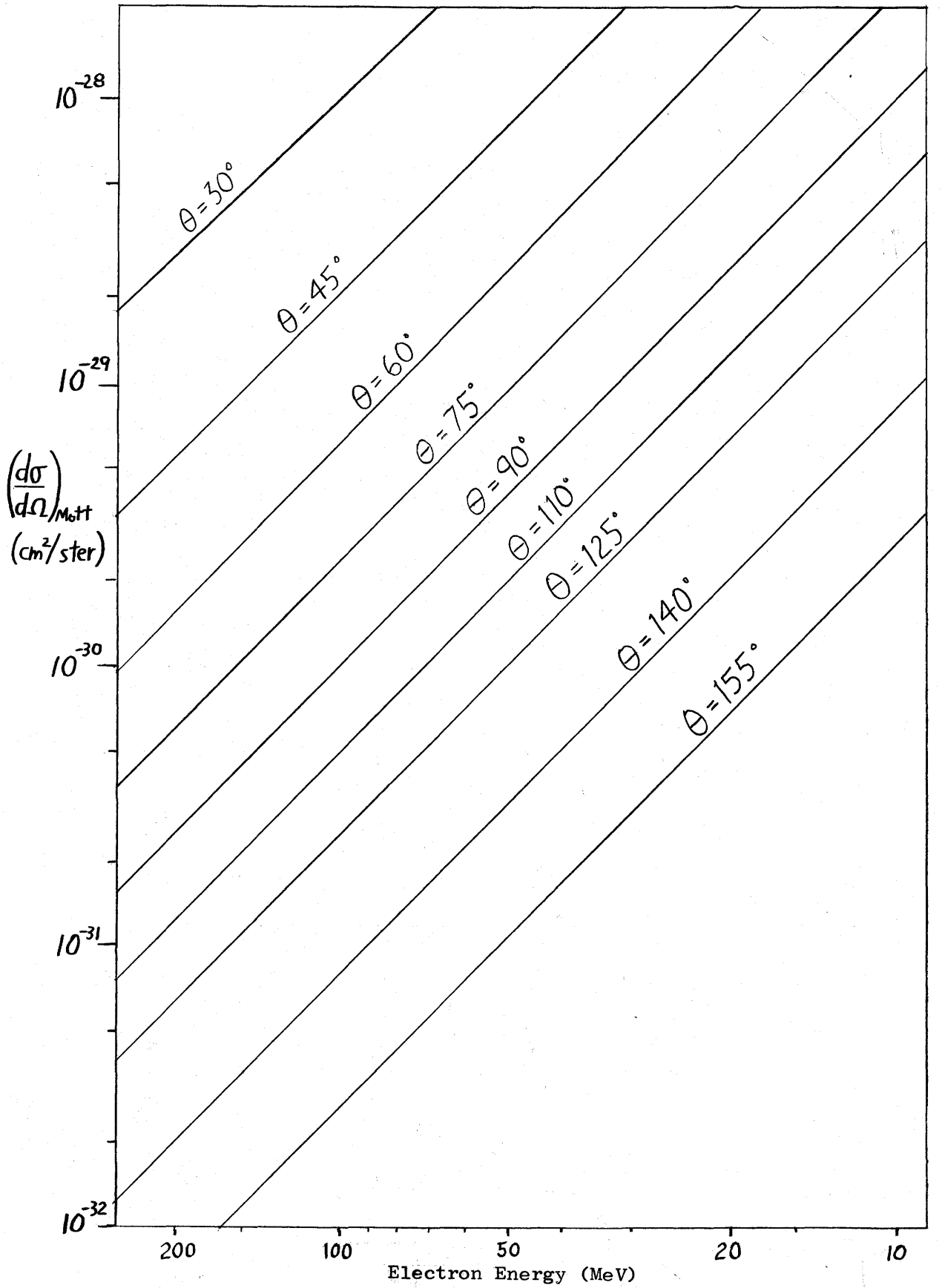

Fig. 5.1 Mott cross section for Z=1, neglecting center-of-mass correction.

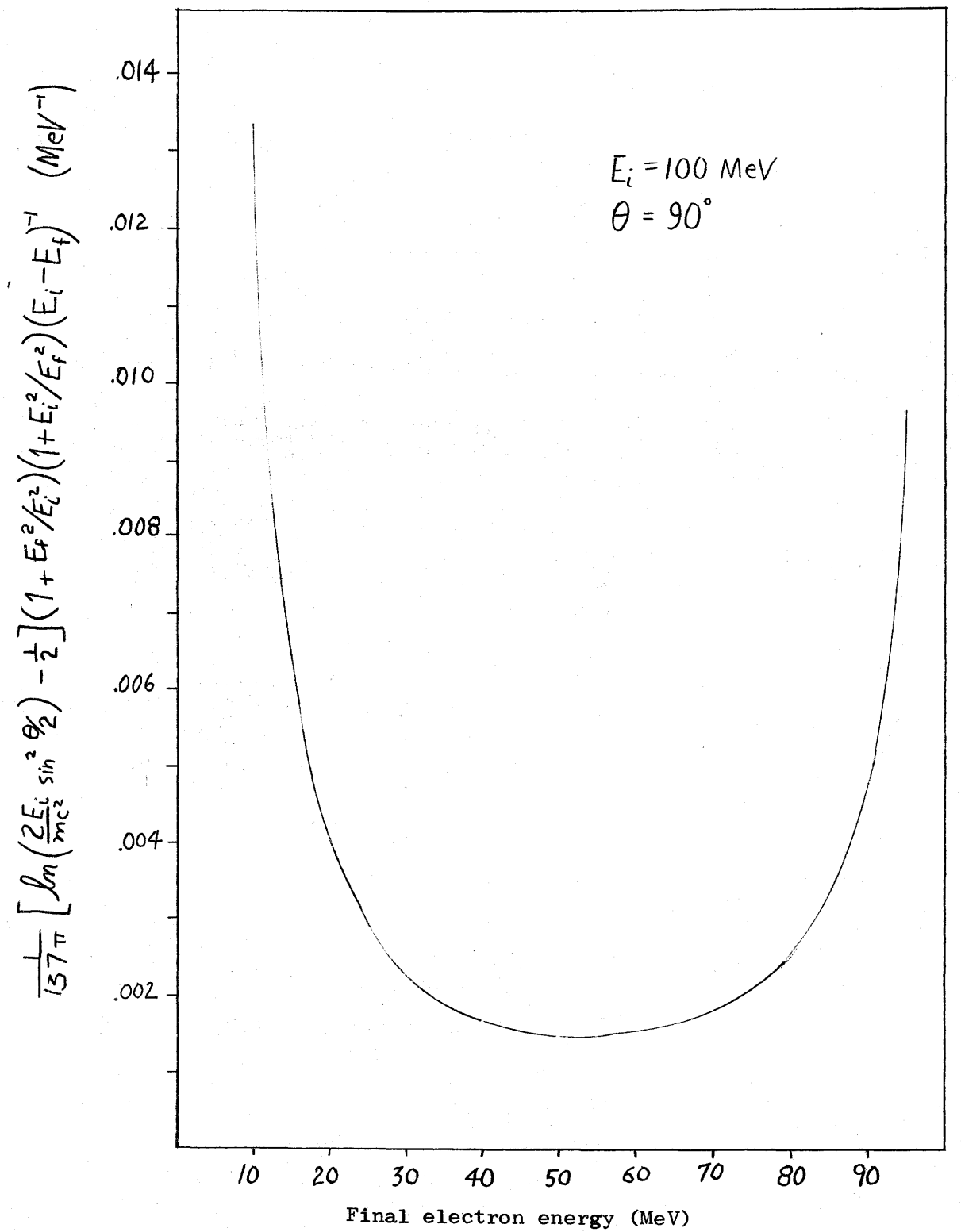

Fig. 5.2 Ratio of Schiff's expression for the radiation tail to the elastic scattering cross section.

as a function of E_f for E_i = 100 MeV, $\theta = 90^o$. Elastic form factors have been set equal to 1.0.

Type II background: The electron undergoes a single large-angle elastic scattering, but a photon is radiated when the electron is accelerated in the electromagnetic field of another nucleus. Isabelle and Bishop (1963) give an expression for this background:

$$\left(\frac{d^2\sigma}{d\Omega\, dE_f}\right)_{II} = \frac{1}{2} t \left(1 + \frac{E_i^2}{E_f^2} \frac{F^2(q_f)}{F^2(q_i)}\right) \left(\frac{1}{X_o} \varphi_{rad}(E_i, E_f)\right) \left(\frac{d\sigma}{d\Omega}\right)_{elastic} \qquad (5.3)$$

where t is the target thickness in gm/cm^2 and X_o is the radiation length of the target material in gm/cm^2. $\varphi_{rad}(E_i, E_f)$ is a function which may be found in Rossi (1952), page 51.

Type III background: The electron undergoes a single large-angle elastic scattering, but loses energy in collisions with atomic electrons in the target. The expression for this may also be found in Isabelle and Bishop (1963). It is

$$\left(\frac{d^2\sigma}{d\Omega\, dE_f}\right)_{III} = \frac{1}{2} t \left(0.3 \frac{Z}{A} \frac{mc^2}{E_i^2} \frac{(E_i^2 - E_i E_f + E_f^2)^2}{(E_i - E_f)^2 E_f^2}\right)$$

$$\times \left(1 + \frac{E_i^2}{E_f^2} \frac{F^2(q_f)}{F^2(q_i)}\right) \left(\frac{d\sigma}{d\Omega}\right)_{elastic} \qquad (5.4)$$

Type IV background: Electrons may reach the detector after scattering from some part of the system other than the target. In addition, particles other than high energy electrons may cause the detectors to give counts. These are effects which depend more on the nature of the beam handling and electron detection systems than on the target. It is very hard to estimate the amount of this type of background; as a guide to what may be expected, the experiences of other electron scattering laboratories are summarized.

At the High Energy Physics Laboratory at Stanford some background was due to electrons which were scattered from the target, onto the wall of the scattering chamber opposite the spectrometer, and then into the spectrometer. The addition of 3 cm. of paraffin inside the chamber wall reduced the background somewhat (Barber et al. (1960). As one would expect, the relative importance of this background decreased as the scattering angle decreased, since for small scattering angle the spectrometer would "see" a part of the chamber wall upon which fewer electrons were scattered from the target. This cause of background is difficult to distinguish from type I background, since its dependence upon target thickness should be nearly the same as that of type I.

At the Laboratoire de l'Accélérateur Linéaire at Orsay, where Cerenkov counters were used to detect electrons, the presence of a Faraday cup in the beam resulted in background due to neutron-induced gamma rays (Isabelle and Bishop (1963)). Such background can be reduced by having the beam stopped as far away as possible from the spectrometer and by increasing the shielding around the detectors.

At the Institut für Technische Kernphysik der Technischen Hochschule, Darmstadt it was found that some electrons were reaching the detector after being scattered from the vacuum chamber walls of the spectrometer. They could be seen as "ghost peaks" at spectrometer settings corresponding to electron energies higher than the energy of the incident beam.

The following numbers obtained at Darmstadt (Titze (1964)) are an indication of the order of magnitude of type IV background:

1) with a target in the beam, spectrometer set above the elastic peak, 0.9 counts/microcoulomb,

2) with no target, spectrometer set above the elastic peak, 0.24 counts/

microcoulomb ,

3) with a target in the beam, spectrometer turned off, 0.56 counts/microcoulomb ,

4) with no target, spectrometer turned off, 0.24 counts/microcoulomb.

Background due to the radiative tail of inelastic peaks (Isabelle and Bishop (1963)) will not be considered in this work. It can be ignored if inelastic peaks are small compared to the elastic peak, as they will be for the cases we shall consider. However, it is an important correction for 180^{o} electron scattering, as can be seen in figure 4 of Goldemberg and Barber (1964), for example.

§2 Quasi-elastic scattering

It has been assumed that the inelastic electron scattering cross section at some particular excitation energy can be represented by one or two terms in the multipole expansion (equation 3.1). At low values of excitation energy, where nuclear levels are well spaced, this is a proper assumption. For a higher excitation energy it may be that many multipoles have to be considered, so that a description of the cross section in terms of multipoles becomes useless. One element for which this has been found to be true is C^{12} (Barber (1962)). Since we shall be interested in 35 MeV excitation of C^{12}, further consideration of quasi-elastic scattering is necessary.

At higher values of momentum transfer an extended bump is seen in inelastic scattering spectra (figure 5.3). This bump is attributed to what has been called quasi-elastic scattering. The importance of quasi-elastic scattering increases with increasing momentum transfer. In the 180^{o} scattering at 70MeV by Goldemberg and Barber (1964) there is little evidence of quasi-elastic scattering. Leiss and Taylor (1960) scattered electrons from C^{12} at an angle of

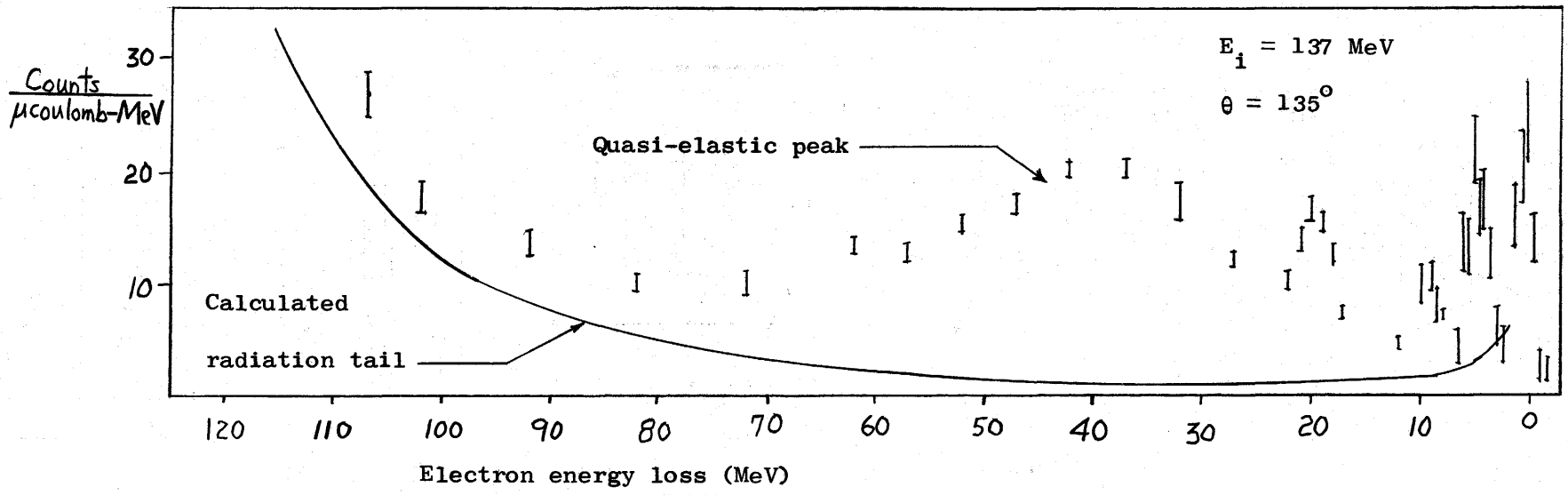

Fig. 5.3 Quasi-elastic scattering contribution to the inelastic spectrum of C^{12} obtained by Leiss and Taylor.

135^{o} with incident electron energies from 80 MeV to 150 MeV. As momentum transfer increased, the quasi-elastic peak increased in height and width. At the highest energy, 147 MeV, it became higher than the elastic peak. Bounin and Bishop (1961) scattered 194 MeV electrons from C^{12} and found the broad peak extending from final electron energies of 30 MeV to 180 MeV.

Attempts have been made to explain the bump in terms of a harmonic oscillator model of the nucleus. The predicted spectrum did not fit the height or position of the peak of Bounin and Bishop (1961), although the shape was good. The harmonic oscillator model gave a cross section which was a factor of 4 smaller than the quasi-elastic peak in Be^{9} (Nguyen Ngoc and Perez y Jorba (1964)). A more correct theory appears to be that the electrons are scattered incoherently from single nucleons. The width of the peak should reflect the momentum distribution of nucleons in the nucleus. Unfortunately, there does not appear to be a theory which can accurately predict the quasi-elastic cross section as a function of incident energy and scattering angle.

Chapter 6

SOME PARTICLE-HOLE MODEL PREDICTIONS CONCERNING DIPOLE EXCITED STATES

§1 The giant resonances of C^{12} and O^{16}

This section is a brief review of applications of the particle-hole model to excited states of closed shell nuclei. It is intended that these examples should make clear the area in which the model is most useful, and what additional experimental data would be desirable.

The outstanding success of the particle-hole model has been the prediction of a dip in the giant resonance cross section for electron scattering as a function of momentum transfer. The results for the giant resonance of C^{12} obtained by Lewis and Walecka (1964) are shown in figure 6.1. The point at a momentum transfer of 115 MeV/c comes from Goldemberg and Barber (1964). This clearly demonstrates the superiority of the particle-hole model over the older hydrodynamic models of Goldhaber and Teller and of Steinwedel and Jensen. On the other hand none of the choices for residual interaction gives a really close fit to experimental results. In the case of the lowest energy dipole state in C^{12}, the particle-hole model gives quite different results for zero-range and Yukawa well residual interactions. The experimental data come close to fitting the matrix element vs. momentum transfer curve for the Yukawa type interaction. This case also demonstrates the limitations of the simple particle-hole model. The model gives only one 1^-, T=1 state of C^{12} below 20 MeV excitation energy. In 180^o scattering at Stanford one peak was seen at an energy of 18 MeV to 19 MeV, however, higher resolution work at Darmstadt revealed peaks at 19.5 MeV and 18.1 MeV. One must now decide whether the 18.1 MeV peak is to be included with the 19.5 MeV peak for purposes of comparison with the model, or whether one of the levels (or possibly even both) is something other than a 1^-,T=1 state.

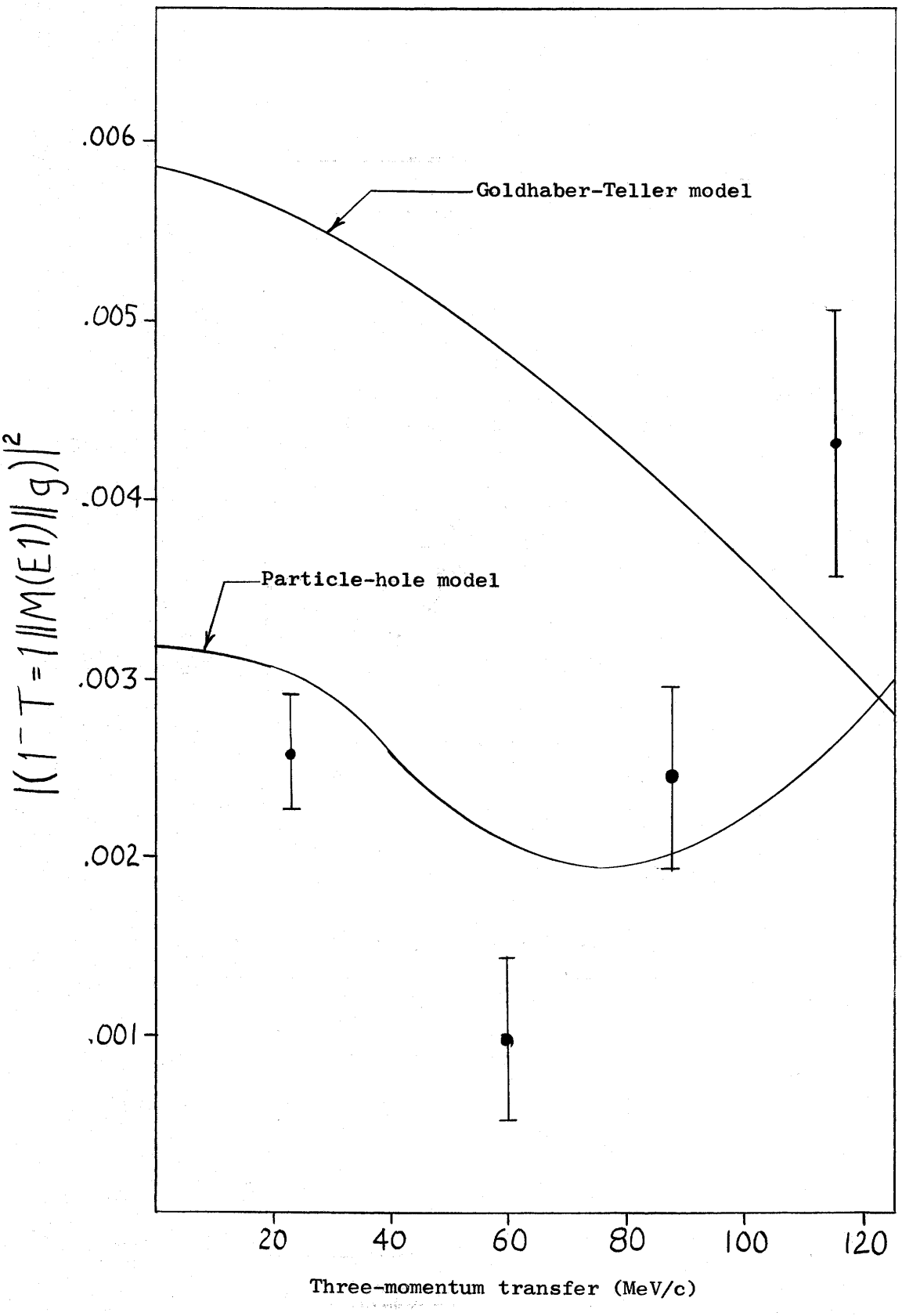

Fig. 6.1 Transverse matrix elements for giant resonance states in C^{12} as calculated by Lewis and Walecka.

Electron scattering measurements on O^{16} show the same sort of behaviour of giant resonance cross section as those on C^{12}. The particle-hole model again predicts a dip in the cross section as a function of momentum transfer and gives a fairly good fit to experimental results. Results of Lewis (1964) and of Vanpraet (1965) are shown in figure 6.2.

The giant resonance of O^{16} also shows the inability of the particle-hole model to explain results of high resolution experiments. The model predicts two peaks between 20 MeV and 25 MeV excitation energy, while experimental evidence indicates at least four peaks in this interval (Tanner, Thomas, and Earle(1964)).

The combinations of energy and current available on the Saskatchewan linear accelerator make it possible to consider fairly high resolution inelastic scattering with momentum transfers of up to 225 MeV/c. It should be possible to check certain other particle-hole model predictions more readily than can be done at other laboratories. One such prediction concerns a dipole excited state in C^{12} with excitation energy approximately 35 MeV. Another region of interest is the giant resonance of Si^{28}. These cases are considered in the following two sections.

§2 A 35 MeV Dipole State in C^{12}

We shall consider the particle-hole model results of Lewis and Walecka (1964). They took the (1^-, T=1) states of C^{12} to be linear combinations of the independent-particle-model states $|2s_{1/2}, 1p_{3/2}^{-1}\rangle$, $|1d_{5/2}, 1p_{3/2}^{-1}\rangle$, $|1d_{3/2}, 1p_{3/2}^{-1}\rangle$, and $|1p_{1/2}, 1s_{1/2}^{-1}\rangle$. The residual interaction which best fitted electron scattering data was found to be one with a Yukawa-type radial dependence and a Serber mixture of exchange terms. One of the eigenvalues of the resulting 4 x 4 Hamiltonian matrix is at 35.8 MeV. The corresponding eigenfunction is

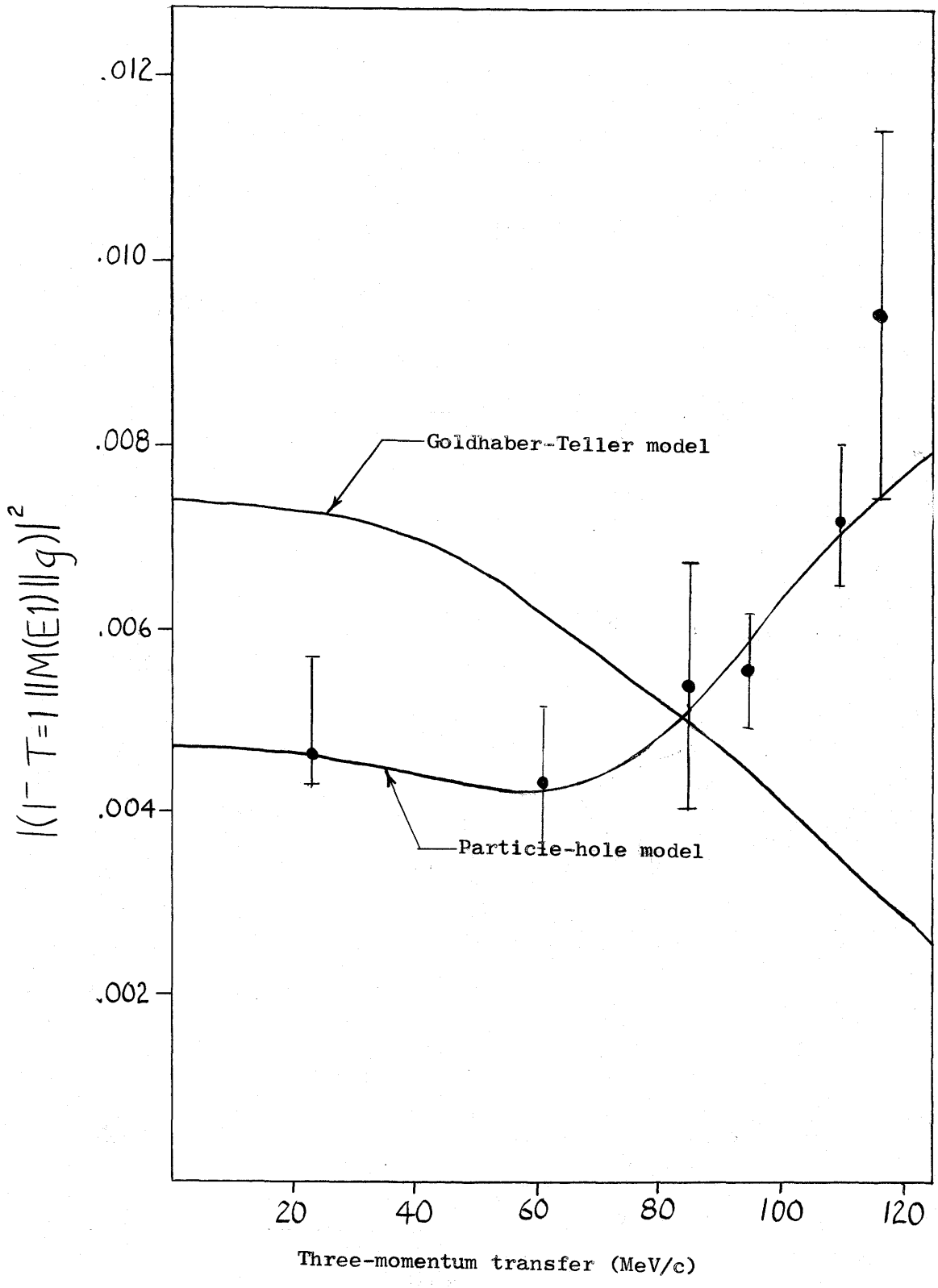

Fig. 6.2 Transverse matrix elements for giant resonance states in O^{16} as calculated by Lewis.

$$|(35\,\mathrm{MeV})\,1^-,T=1\rangle = -0.027\,|2s_{1/2}\,1p_{3/2}^{-1}\rangle - 0.044\,|1d_{5/2}\,1p_{3/2}^{-1}\rangle$$
$$+ 0.260\,|1d_{3/2}\,1p_{3/2}^{-1}\rangle + 0.964\,|1p_{1/2}\,1s_{1/2}^{-1}\rangle. \qquad (6.1)$$

From chapter 3 we obtain expressions for matrix elements $\langle(\alpha\bar{\beta})\lambda T0\|M(C\lambda)\|g\rangle$ and $\langle(\alpha\bar{\beta})\lambda T0\|M(E\lambda)\|g\rangle$. The results are

$$\left|\langle(35\,\mathrm{MeV})\,1^-T=1\|M(C1)\|g\rangle\right|^2 = 0.0580\,q^2 e^{-1.39q^2}\left[1.-0.066q^2\right]^2 \qquad (6.2)$$

and

$$\left|\langle(35\,\mathrm{MeV})\,1^-T=1\|M(E1)\|g\rangle\right|^2 = 0.000786\,e^{-1.39q^2}\left[1.+6.00q^2-0.49q^4\right]^2 \qquad (6.3)$$

where the three-momentum q is measured in inverse fermis. The correction terms for center-of-mass motion and finite size of nucleons have been included, but the Darwin term has been omitted in the expression for the coulomb matrix element. The two matrix elements have been plotted as a function of momentum transfer in figure 6.3.

The particle-hole model predicts that for transverse excitation this level should be as strong as the giant dipole resonance at q = 90 MeV/c. At q = 23 MeV/c it should be about one-third as large as the giant resonance. There is considerable evidence that there is an excited state in this energy region, however, little of it comes from electron scattering work. Most of the spectra are of low resolution or consist of only a few measured points.

A number of reactions have been used to study excited levels of C^{12}. In a study by Vanhuyse and Barber (1961) of photoprotons from C^{12}, a level at about 36 MeV was indicated. Their results, reproduced in figure 6.4, show the desirability of a measurement at higher resolution. The $C^{12} + \gamma \longrightarrow 3\alpha$ cross section measured by Maikov (1958) shows one or possibly two levels between 34 MeV and 36 MeV excitation energy. Taran and Gorbunov

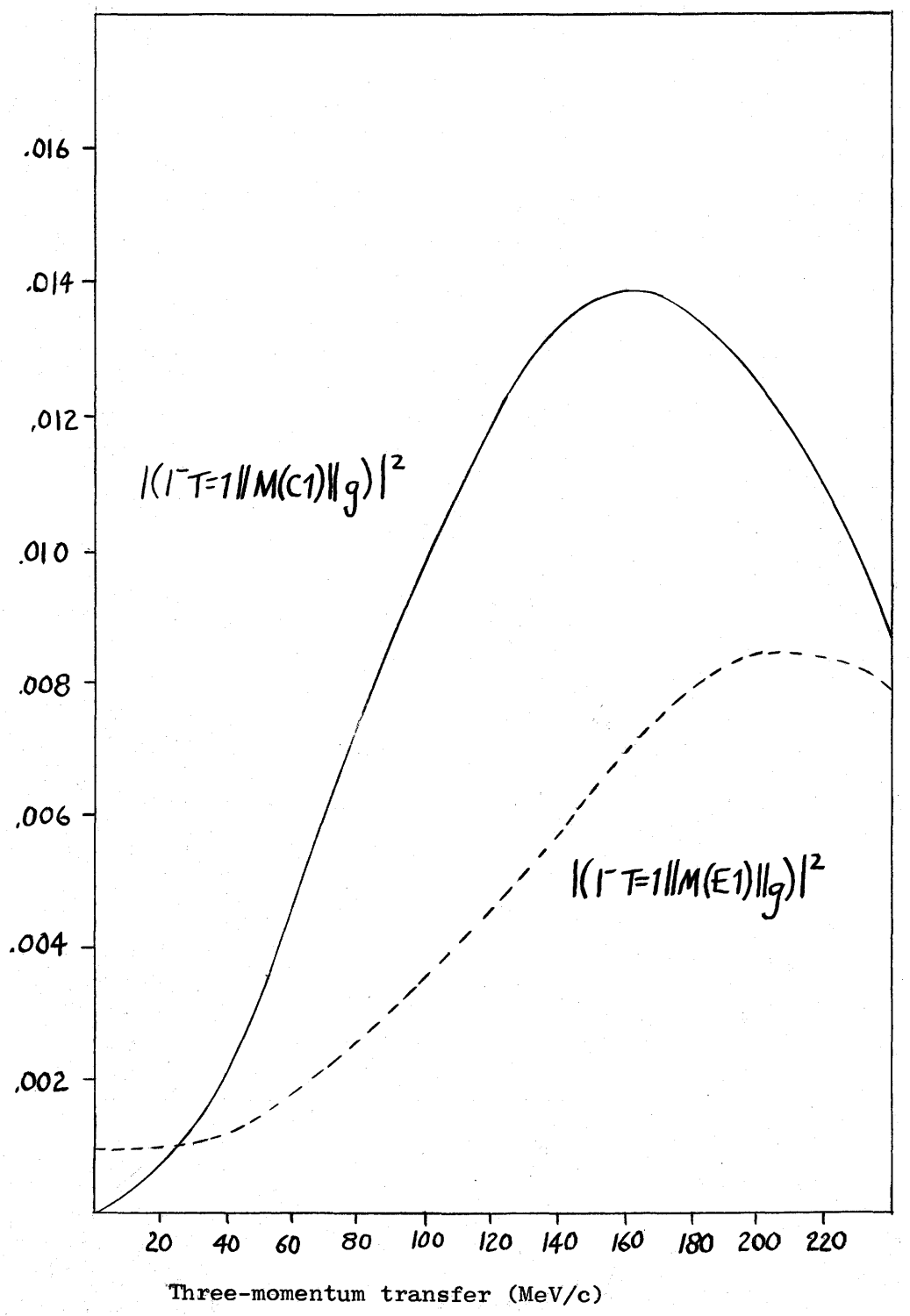

Fig. 6.3 Matrix elements for a particle-hole state at 35 MeV in C^{12}.

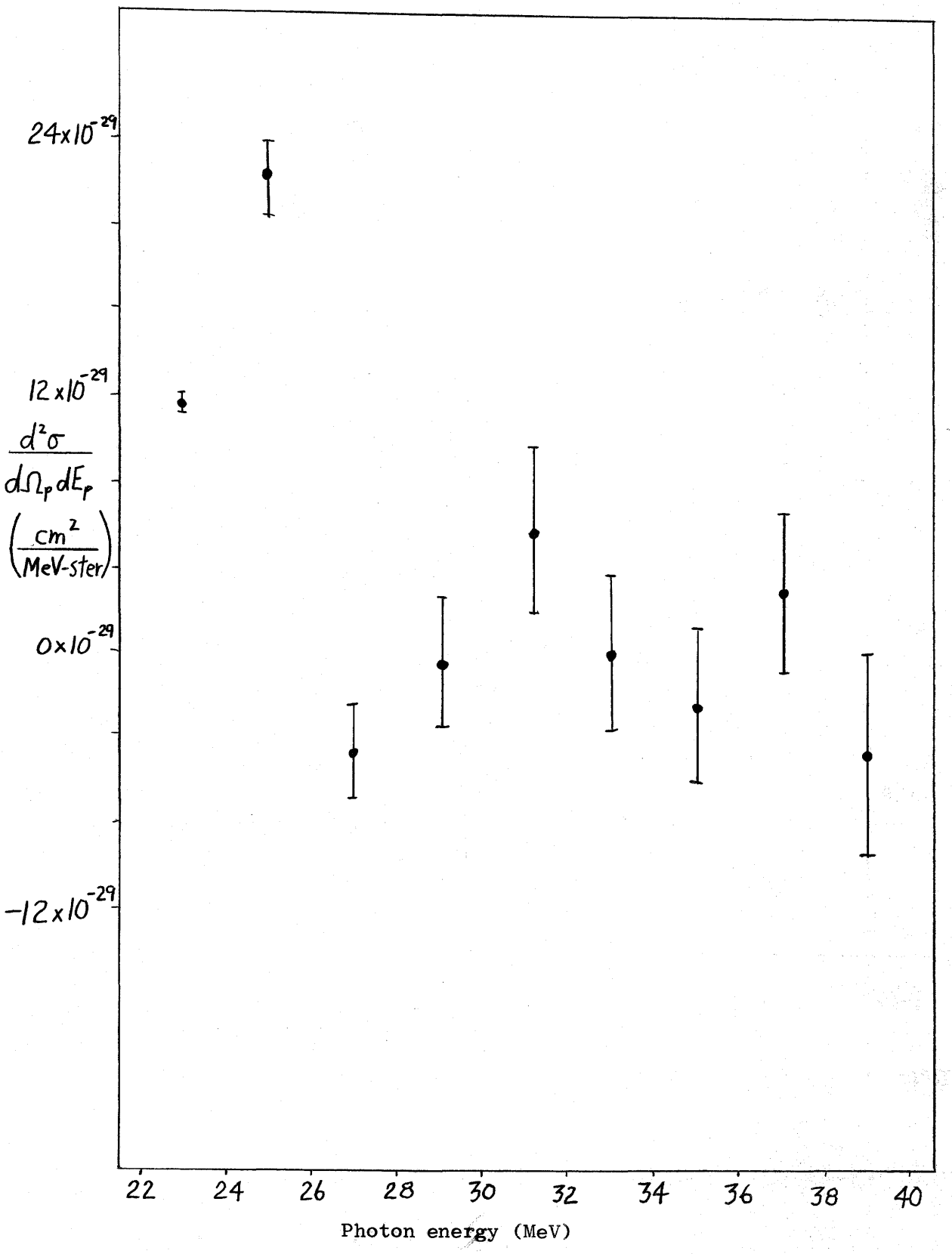

Fig. 6.4 $C^{12}(\gamma,p)B^{11}$ cross section obtained by Vanhuyse and Barber by photon difference analysis.

(1964), studying the $C^{12}(\gamma,p)B^{11}$ reaction, found a level at 34.5 MeV which they identified with the particle-hole model dipole state predicted by Vinh-Mau and Brown (1962). Reay, Hintz, and Lee (1963) have studied the inverse reaction $B^{11}(p,\gamma)C^{12}$. They found a level at a proton energy corresponding to 35 MeV excitation energy of the C^{12} nucleus.

Most of the published electron scattering data consist of spectra with few measured points in the energy region of 35 MeV. Typical spectra are those of Leiss and Taylor (1960). The most useful results probably are from 180^{o} scattering by Goldemberg and Barber (1964). The spectrum in their figure 4 indicates at least one level in the energy range of interest, however, it is much smaller, relative to the levels near 23 MeV, than is predicted by the particle-hole model.

§3 Dipole States of Si^{28} between 15 MeV and 25 MeV

In a j-j coupling scheme Si^{28} has no partially-filled neutron or proton shells, so it is reasonable to use the particle-hole model to describe 1^{-},T=1 excited states of this nucleus. Seaborn and Eisenberg (1965) have done this, taking seven particle-hole configurations into account. They tried two values, differing by about 9%, for the strength of the residual interaction, which was a zero-range type. Ground state correlations were neglected. For each of the seven particle-hole dipole states a quantity proportional to the square of the matrix element was plotted as a function of momentum transfer. The transverse matrix elements of five of these states go through zeroes for values of momentum transfer which can be attained using the Saskatchewan linear accelerator. The particle-hole model also predicts the excitation energies of the levels and their relative strengths as a function of momentum transfer. The two values of residual interaction

give appreciably different values for excitation energies and relative strengths of two levels near 18 MeV and 21 MeV (see figures 6.5 and 6.6). Electron scattering should make it possible to determine the extent to which the simple particle-hole model describes the giant resonance of Si^{28}. Should the particle-hole model prove accurate, it might be possible to determine the correct value for the strength of the residual interaction.

The matrix elements obtained by Seaborn and Eisenberg (1965) are shown in figures 6.5, 6.6, and 6.7. Their definition of a matrix element differs from the one used in this thesis by a factor $[(2J_f+1)/(e^2/hc)]^{\frac{1}{2}}$. In order to keep a consistent definition of matrix elements, the ordinates in figure 1 of Seaborn and Eisenberg (1965) have been multiplied by $(2J_f+1)\alpha^2/36\pi M^2 = 3.8 \times 10^{-3}$ and those of figure 2 by $(2J_f+1)/36\pi = 2.65 \times 10^{-2}$.

Two papers with results of inelastic electron scattering from Si^{28} are Barber et al. (1960) and Stoval et al. (1965). The latter group measured the transition strength integrated from 13 MeV to 27 MeV for momentum transfer values 153 MeV/c and 223 MeV/c. Their results are in good agreement with particle-hole model predictions. However, as Seaborn and Eisenberg (1965) point out, this integration tends to obscure details of the model. The sum of transition strengths of all dipole states depends upon the wave function of the ground state, but not upon those of the excited states (because of the dipole sum rule). Integration from 13 MeV to 27 MeV probably includes most of the dipole strength. More information could be gained by determining the behaviour of individual levels within this energy range.

$Al^{27}(p,\gamma)Si^{28}$, $Si^{28}(\gamma,p)Al^{27}$, and $Si^{28}(\gamma,\alpha)Mg^{24}$ reactions have been used to look at the structure of the giant resonance of Si^{28}. In general, the results do not favor the particle-hole model. Cannington et al. (1965) measured $Si^{28}(\gamma,p)Al^{27}$ and $Si^{28}(\gamma,\alpha)Mg^{24}$ cross sections with a resolution

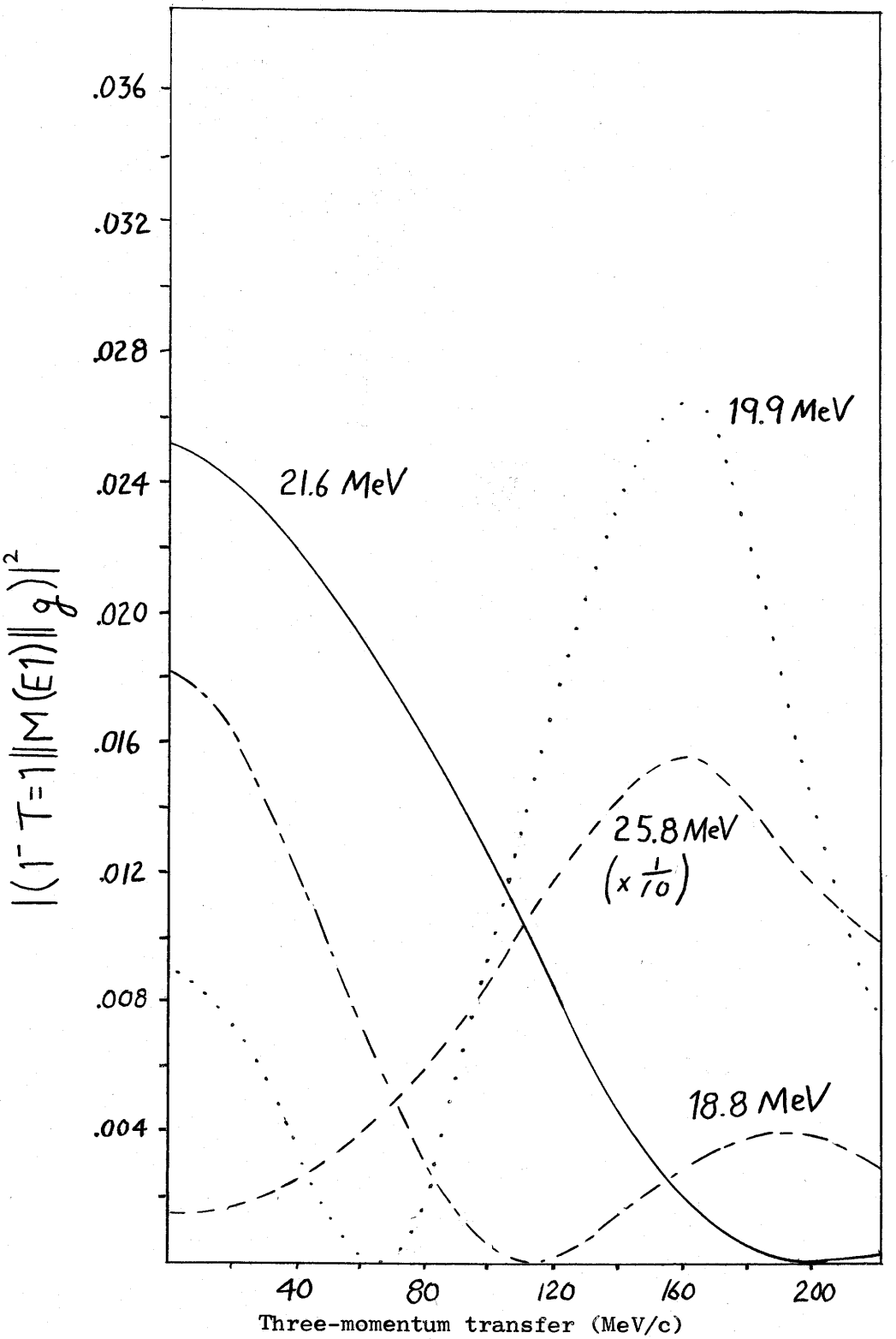

Fig. 6.5 El matrix elements of Si^{28} as calculated by Seaborn and Eisenberg. Strength of residual interaction is 10.92 MeV.

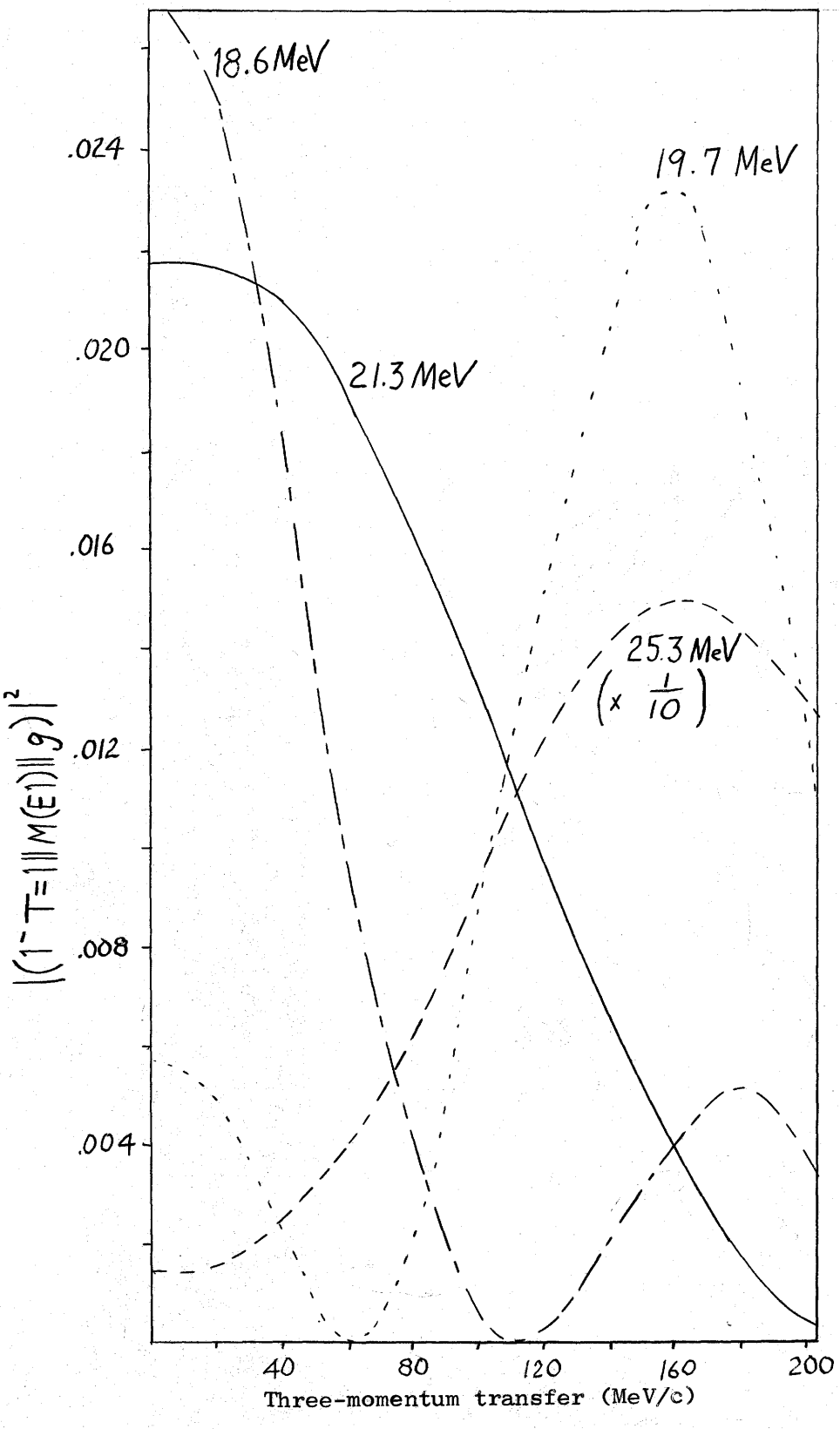

Fig. 6.6 El matrix elements of Si^{28} as calculated by Seaborn and Eisenberg. Strength of residual interaction is 10.00 MeV.

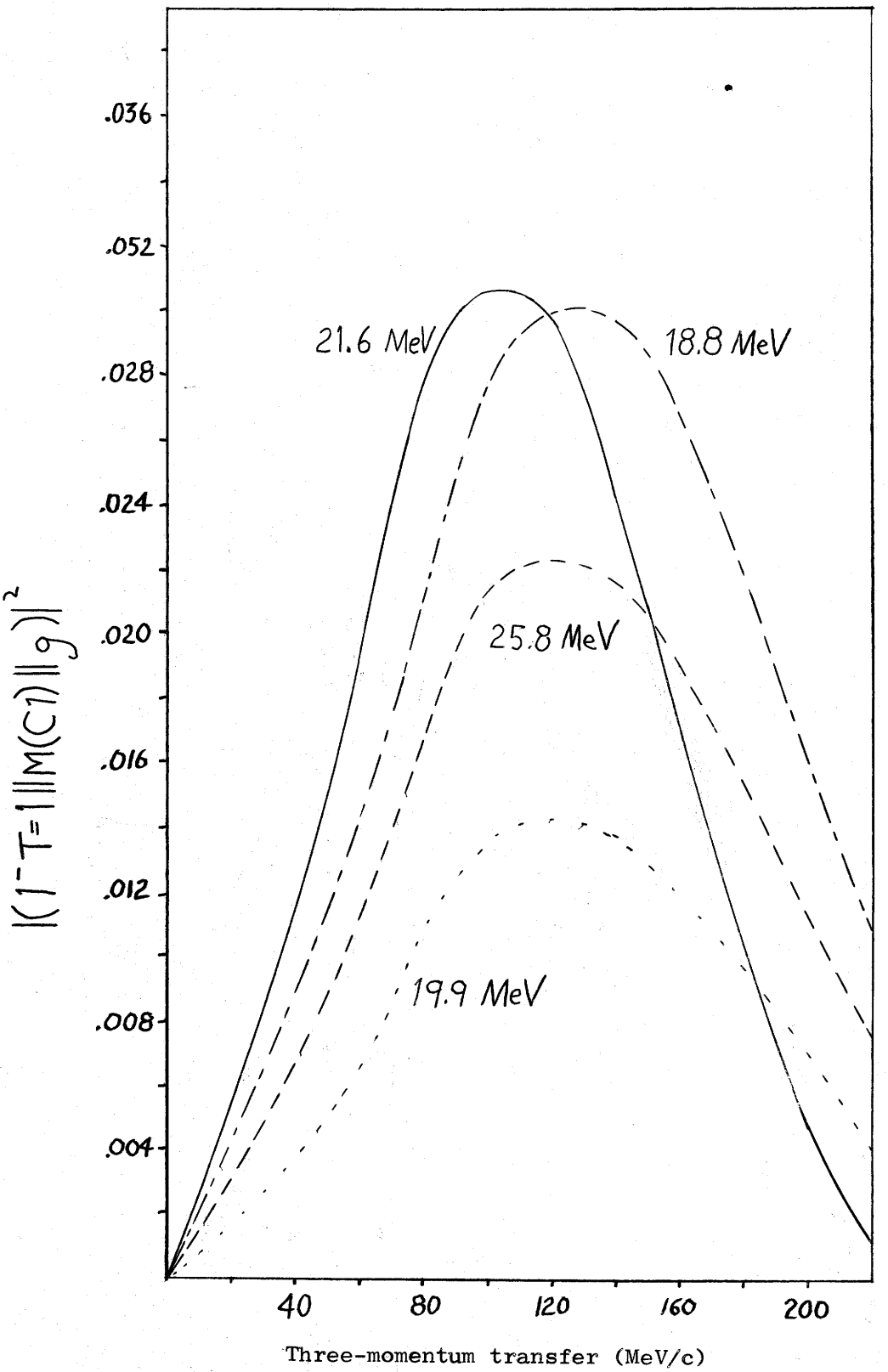

Fig. 6.7 C1 matrix elements of Si^{28} as calculated by Seaborn and Eisenberg. Strength of residual interaction is 10.92 MeV.

of about 70 keV. They found more levels than the particle-hole model predicted, and in particular found a strong state at 18.0 MeV which could not be matched with any particle-hole model level. Singh et al. (1965) found that the particle-hole model could not explain the results of their measurements of $Al^{27}(p,\gamma)Si^{28}$ cross sections. They found a large number of narrow peaks superimposed on the coarse structure of the giant resonance. Their analysis showed that these peaks could be interpreted as Ericson fluctuations. They also found that the angular distribution of gamma rays varied little with the energy of the excited state; calculations based on the particle-hole model predicted that the angular distribution should vary markedly with energy of the excited state. Bizzeti et al. (1965) studied the $Si^{28}(\gamma,p)Al^{27}$ and $Si^{28}(\gamma,\alpha)Mg^{24}$ cross sections. Using gamma rays from the Li^{7} + p reaction, they were able to achieve a resolution of 12 keV with an energy range of about 100 keV around 17.6 MeV. They found six transitions which might be interpreted as Ericson fluctuations.

Chapter 7

ESTIMATES OF COUNTING RATES AND BACKGROUNDS

§1 Choice of Target Thickness

In choosing the thickness of target, one must compromise between low counting rates which result from thin targets, and the loss of resolution which results from thicker targets. Thechoice of target thickness will depend upon factors such as long term energy stability of the accelerator and spectrometer and the amount of accelerator time available for the experiment. Since it is very difficult to estimate such factors at this time, the discussion of target thickness must be in rather general terms.

It is useful to consider the dependence upon target thickness of the various types of background which were discussed in chapter 5, §1. The counting rate due to excitation of a nuclear dipole state, which is proportional to target thickness t, must be observed above this background. The counting rate due to type I background is also proportional to t, while type II and type III background is proportional to t^2. It is to be expected that type IV background will be partly independent of t and partly proportional to t. Figure 7.1 shows the form of the dependence of background cross section upon target thickness for the different types of background. As was mentioned in the previous paragraph, it is very hard to estimate the factors which determine the lower limit to target thickness. To set an upper limit, a useful number to know is t_o, the thickness for which $\left(\frac{d^2\sigma}{d\Omega dE_f}\right)_I = \left(\frac{d^2\sigma}{d\Omega dE_f}\right)_{II} + \left(\frac{d^2\sigma}{d\Omega dE_f}\right)_{III}$. For scattering from C^{12} with E_i = 100 MeV, E_f = 70 MeV, and $\theta = 90^o$, we get t_o = 3.7 gm/cm^2. t_o is nearly independent of scattering angle for θ between 30^o and 150^o.

When we are dealing with large excitation energies, another effect of having a thick target becomes more important than type II and type III

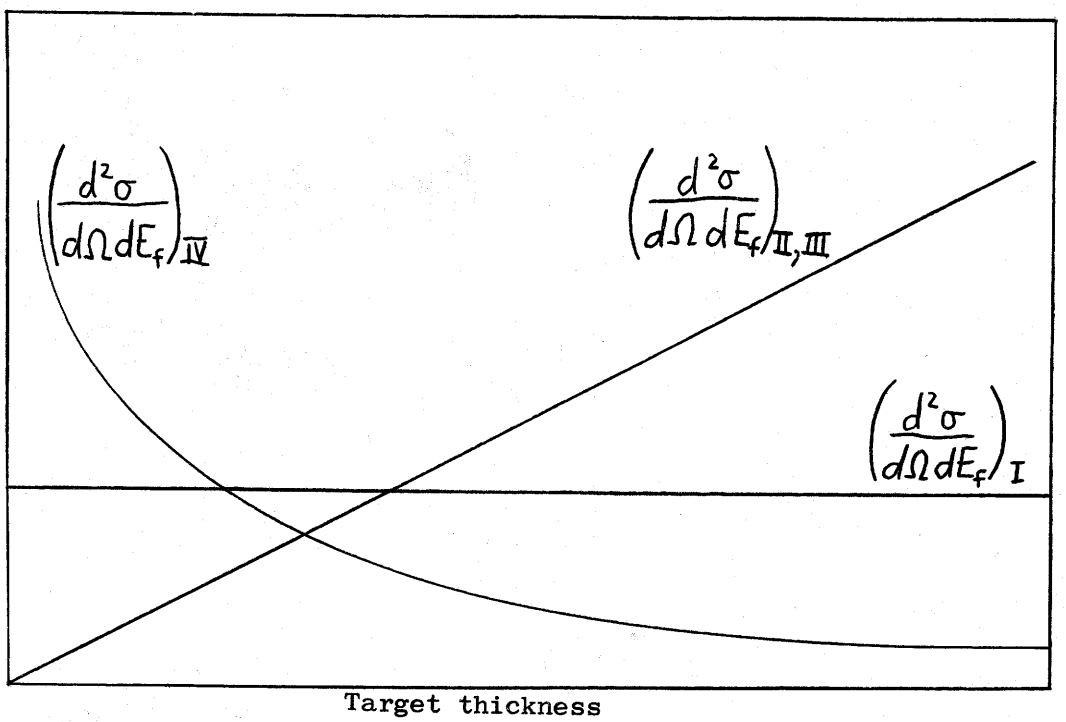

Fig. 7.1 Form of the dependence upon target thickness of various types of background.

background. This effect is the loss of resolution due to broadening of peaks, which results from statistical fluctuation in the ionization losses of scattered electrons in the target. An expression relating width of the energy distribution to target thickness is given by Bethe and Ashkin (1953)(as quoted in Appendix I of Elliott (1964)):

$$\delta E = 3.98\ (2\pi e^4 nt)/(mc^2 \rho \beta^2), \qquad (7.1)$$

where n is the number of atomic electrons per cm^2 of the target,

ρ is the density of the target in gm/cm^3,

t is the target thickness in gm/cm^2,

δE is the full-width-at-half-maximum (in MeV) of the energy distribution, and where the other symbols have their usual meaning.

For a graphite target this gives $\delta E \simeq 0.3t$ if we assume $\beta \simeq 1$. It is desir-

able to keep δE less than the corresponding width of the energy distribution of incident electrons. A reasonable, if somewhat arbitrary, upper limit on δE is 50 keV. This sets an upper limit to target thickness of $t \simeq 170$ mg/cm^2.

§2 Detector Dead Time Losses on the Elastic Peak

When targets are thick enough to give adequate counting rates for inelastic scattering, it may be possible to have average counting rates the order of one per pulse on the elastic peak. If the detection and counting system has a dead time which is not small compared to the average interval between events, it is necessary to consider counting losses due to dead time. If the detection system is capable of giving no more than one count per pulse, the correction is particularly simple. If $\bar{p}$ is the average number of electrons reaching the detector per pulse, the average number of counts per pulse is

$$\bar{r} = 1 - \exp(-\bar{p}). \tag{7.2}$$

In Appendix C it is shown that the statistical error is minimized by choosing beam current to give an average counting rate $\bar{r} = 0.8$ per pulse when such a detector is used.

§3 Backgrounds and Counting Rates for Various Combinations of Incident Energy and Scattering Angle

To obtain peak counting rates and backgrounds it is necessary to make certain assumptions and approximations. The assumptions and approximations used in this section are:

1) The contribution to the inelastic cross section of the 35 MeV level in C^{12} is $\frac{d^2\sigma}{d\Omega dE_f} = \frac{d\sigma}{d\Omega} \div 1\,MeV$ at the peak. This introduces the greatest uncertainty into the calculations and the assumption may easily be in error by a

factor of two. However, the particle-hole model does not predict level widths and experiments have not been done with sufficiently high resolution to indicate a level width. The cross sections of Si^{28} were divided by a factor of 0.5 MeV. This seemed reasonable in view of the widths obtained by Cannington et al. (1965) for peaks in the (γ,p) and (γ,α) cross sections.

2) The coefficients of longitudinal and transverse matrix elements may be expressed by their values in the limit $k_f \rightarrow k_i$. We have

$$\lim_{k_f \to k_i} 4\pi \left(\frac{4k_i k_f \sin^2(\theta/2)}{q^2} \right)^2 = 4\pi$$

and

$$\lim_{k_f \to k_i} 4\pi \left(\frac{k_i^2 + k_f^2 + 2k_i k_f \sin^2(\theta/2)}{q^2} \right) = 4\pi \left(\frac{1}{2} + \tan^2 \frac{\theta}{2} \right).$$

This makes the expressions for multipole cross sections which are used in this section

$$\frac{d\sigma_{C\lambda}}{d\Omega} = 4\pi \frac{1}{2J_i+1} \left| (f \| M(C\lambda) \| i) \right|^2 \left(\frac{d\sigma}{d\Omega} \right)_{Mott, Z=1} \qquad (7.3)$$

and

$$\frac{d\sigma_{E\lambda}}{d\Omega} = 4\pi \left(\frac{1}{2} + \tan^2 \frac{\theta}{2} \right) \frac{1}{2J_i+1} \left| (f \| M(E\lambda) \| i) \right|^2 \left(\frac{d\sigma}{d\Omega} \right)_{Mott, Z=1} \qquad (7.4)$$

The error introduced by this approximation is most serious for small scattering angles. For $\theta = 45^\circ$ and $k_f/k_i = 2/3$ the error in $\frac{d\sigma_{C\lambda}}{d\Omega}$ is 30% of the proper value, while for $\frac{d\sigma_{E\lambda}}{d\Omega}$ the error is 20%.

3) The background is assumed to be entirely type I background, with $\left(\frac{d^2\sigma}{d\Omega\, dE_f} \right)_I$ given by the expression of Schiff. The expression of Maximon and Isabelle (1964) for type I background, which should be more accurate, varies between 0.6 and 1.0 of the Schiff expression for angles between 45° and 150° (see their figure 2). For target thicknesses below 200 mg/cm^2 and high excitation energies types II and III background should be negligible, however, the same cannot be said for background of type IV. The effect of neglecting $\left(\frac{d^2\sigma}{d\Omega\, dE_f} \right)_{IV}$

will be to cancel some of the error which arises from using the Schiff expression for $\left(\frac{d^2\sigma}{d\Omega dE_f}\right)_I$.

4) Nuclear recoil energy is neglected. The E_f should be slightly smaller, which would in general give a larger value of q as well as causing slight changes in the calculated cross sections. The correction to E_f following an elastic scattering is a factor $(1 + (2E_i/AM)\sin^2\frac{1}{2}\theta)^{-1}$, which is 0.8 for E_i = 125 MeV and $\theta = 150^\circ$.

5) The only nuclear levels being excited are 1^-, T=1 levels and their cross sections are given by the particle-hole model.

6) The operating conditions are the "standard conditions" given in table 7.1.

Table 7.1 Parameters used in calculation of backgrounds and counting rates. Symbols are defined following equation 4.2.

Parameter	For C^{12} target	For Si^{28} target
ΔE_f	0.2 MeV	0.1 MeV
$\Delta\Omega$	5×10^{-3} ster	5×10^{-3} ster
$\frac{\rho t}{A} \sec\frac{1}{2}\theta$	1×10^{-2} cm^{-2}	5×10^{-3} cm^{-2}
i_{avg}	2 μA	1 μA

This gives $\dot{n} = 7.5 \times 10^{3} \frac{\text{MeV-ster}}{\text{cm}^2\text{-sec}} \cdot \frac{d^2\sigma}{d\Omega dE_f}$ for C^{12} and $\dot{n} = 9.4 \times 10^{3} \frac{\text{MeV-ster}}{\text{cm}^2\text{-sec}} \cdot \frac{d^2\sigma}{d\Omega dE_f}$ for Si^{28}.

7) The elastic form factor for C^{12} is taken from equation 132 of Hofstadter (1957). This gives $F(q) = (1 - 0.3q^2)\exp(-0.76q^2)$ if q is measured in fm^{-1}. The Si^{28} form factor is from Helm (1956) and is the one resulting from what Helm calls a uniform-uniform charge distribution. The form factor is $F(q) = 3(qR)^{-3}\{\sin qR - qR\cos qR\}3(qu)^{-3}\{\sin qu - qu\cos qu\}$ with R = 3.5 fm and u = 2.2 fm.

8) The counting rates for Si^{28} will be done for the 18.8 MeV state only. Counting rates for other particle-hole states may be obtained by substituting appropriate matrix elements from figures 6.5, 6.6, and 6.7.

We wish to obtain cross sections over a range of values of momentum transfer. In the case of C^{12} it will be desirable to measure the cross section for different angles but the same momentum transfer in order to separate the longitudinal and transverse terms. Table 7.2 gives counting rates and background for combinations of q and θ, calculated for the particle-hole state at 35 MeV excitation energy in C^{12}. Table 7.3 gives similar information for the state in Si^{28} at 18.8 MeV. In both tables $\dot{n}$ includes the contribution of the Schiff term.

Table 7.2 Inelastic scattering cross sections and counting rates for the particle-hole state at 35 MeV in C^{12}.

θ	E_i(MeV)	q(MeV/c)	$\frac{d\sigma_{El}}{d\Omega}\Big/\left(\frac{d\sigma}{d\Omega}\right)_{elastic}$	$\frac{d\sigma_{Cl}}{d\Omega}\Big/\left(\frac{d\sigma}{d\Omega}\right)_{elastic}$	$\left(\frac{d^2\sigma}{d\Omega dE_f}\right)_{Schiff}\Big/\left(\frac{d\sigma}{d\Omega}\right)_{elastic}\left(\frac{1}{MeV}\right)$	$\dot{n}$ (sec^{-1})
155^o	65	95	0.055	0.008	0.004	4.7
155^o	110	180	1.03	0.067	0.005	4.6
155^o	125	210	2.08	0.14	0.007	3.0
125^o	135	210	0.35	0.107	0.005	4.4
125^o	70	95	0.011	0.006	0.004	8.8
45^o	135	95	0.001	0.004	0.002	120.

Table 7.3 Inelastic scattering cross sections and counting rates for the particle-hole state at 18.8 MeV in Si^{28}.

θ	E_i (MeV)	q (MeV/c)	$\frac{d\sigma_{E1}}{d\Omega}\Big/\left(\frac{d\sigma}{d\Omega}\right)_{elastic}$	$\frac{d\sigma_{C1}}{d\Omega}\Big/\left(\frac{d\sigma}{d\Omega}\right)_{elastic}$	$\left(\frac{d^2\sigma}{d\Omega dE_x}\right)_{Schiff}\left(\frac{1}{MeV}\right)\Big/\left(\frac{d\sigma}{d\Omega}\right)_{elastic}$	$\dot{n}$ (sec^{-1})
155°	90	155	0.087	0.039	0.006	0.70
155°	60	100	0.007	0.011	0.009	0.92
155°	30	40	0.022	0.006	0.006	21.
125°	65	100	0.001	0.006	0.004	4.0
45°	55	40	0.000	0.001	0.003	450.
45°	135	95	0.000	0.004	0.003	77

In the case of C^{12} the radiation tail is much smaller than the dipole level which the particle-hole model predicts. The predicted counting rates also are acceptable; for the cases calculated in table 7.2, measurement for 10 minutes at a point on the peak would give at least 1000 counts.

The particle-hole model calculations for Si^{28} in table 7.3 are less encouraging than the results for C^{12}. The background due to radiation tail of the elastic peak is more important, particularly for the 45° scattering. At q = 155 MeV/c we are approaching a zero of the function which we have used for the nuclear form factor, that is, one of the diffraction minima where the Born approximation is inaccurate. It is possible that the calculated form factor is too small, in which case the ratio of dipole cross section to radiative tail would become less favorable, although $\dot{n}$ would not be changed appreciably. It should be noted that the calculations

have been done for values of momentum transfer for which the matrix element is small. Counting rates on other levels might be acceptable for high-energy scattering at 150^{o}. In particular, the level at 25.8 MeV should give counting rates an order of magnitude higher than the ones in table 7.3.

Chapter 8

SUMMARY AND CONCLUSIONS

Inelastic electron scattering can provide a more severe test of a nuclear model than does photoabsorption, since cross sections for excitation of a particular level can be obtained at different values of momentum transfer. Its most serious shortcoming is that electrons may lose energy through processes other than the excitation of nuclei. The accuracy with which inelastic scattering cross sections can be determined is limited by the accuracy in determining the background due to these other processes, particularly in the case of a broad level or series of levels. Because type IV backgrounds for the Saskatchewan accelerator are not known at this time, it is difficult to draw definite conclusions on the feasibility of measuring certain inelastic scattering cross sections. However, unless background found at the Saskatchewan laboratory differs considerably from that found elsewhere, the scattering experiments proposed below should yield useful information.

The particle-hole model calculations of Lewis and Walecka (1964) predict a dipole level in C^{12} at 35 MeV excitation energy. There is considerable evidence for at least one level in this region, but almost all measurements have been made with resolutions of 1 MeV or worse. The electron scattering by Goldemberg and Barber (1964) seems to show that the level at 35 MeV is not as strong as is predicted by the particle-hole model. It appears worthwhile to look for a level near 35 MeV excitation energy by means of electron scattering measurements at fairly high resolution to check particle-hole model predictions. It is suggested that measurements be made at the six combinations of scattering angle and energy of table 7.2. Each spectrum might be obtained with points 0.2 MeV apart in final electron

energy over a region of perhaps 6 MeV centered at 35 MeV. Adequate counting rates should be obtained with a 100 mg/cm^2 thick target. At the higher values of momentum transfer one should expect that quasi-elastic scattering would begin to obscure individual levels in this region of excitation energy.

Seaborn and Eisenberg (1965) have applied the simple particle-hole model to giant resonance states of Si^{28}. There is some difficulty in matching levels predicted by the particle-hole model to levels found in (p,γ) work (Singh et al. (1965)) and (γ,p) experiments (Cannington et al. (1965)), particularly one found at 18 MeV. There appear to have been no high resolution electron scattering experiments done on Si^{28}. Useful combinations of scattering angle and incident energy are 155° and 30 MeV, 155° and 60 MeV, 125° and 65 MeV, and 45° and 135 MeV. For a target thickness of 100 mg/cm^2 predicted counting rates at large energy and scattering angle become less than 1 per second for the 18.8 MeV level. Such low counting rates are undesirable, since long running times are required to obtain a spectrum and general background may give comparable counting rates. The quasi-elastic peak in C^{12} begins at about 30 MeV excitation energy; it is hoped that the same is true for Si^{28}, so that quasi-elastic scattering would not be a problem in the region 15 MeV to 25 MeV.

It would be worthwhile to attempt high resolution measurements over an interval of at least 2 MeV, so that the spectrum could be compared with the results of (γ,p) and (p,γ) experiments involving Si^{28}.

APPENDIX A

REDUCTION OF PARTICLE-HOLE MATRIX ELEMENTS

Let us consider the matrix element

$$\langle n_\alpha l_\alpha j_\alpha m_\alpha m_{t\alpha};\ n_\beta l_\beta j_\beta m_\beta m_{t\beta} | V | n_\gamma l_\gamma j_\gamma m_\gamma m_{t\gamma};\ n_\delta l_\delta j_\delta m_\delta m_{t\delta} \rangle$$

V is of the form $V = \frac{1}{2} \sum_{a,b,c,d} (ab|v|cd)\, a_a^\dagger a_b^\dagger a_c a_d$.

We assume v is symmetric in the variables of integration so that $(\alpha\beta|v|\gamma\delta) = (\beta\alpha|v|\delta\gamma)$. By the orthogonality of states in occupation-number representation (Schweber (1961), page 127), the sum reduces to $a = \alpha$ or $-\delta$, $b = -\delta$ or α and $c = -\beta$ or γ, $d = \gamma$ or $-\beta$. We need consider only four terms in the expression for V:

$$\frac{1}{2}\Big\{(-\delta\alpha|v|-\beta\gamma)\, a_{-\delta}^\dagger a_\alpha^\dagger a_{-\beta} a_\gamma + (-\delta\alpha|v|\gamma-\beta)\, a_{-\delta}^\dagger a_\alpha^\dagger a_\gamma a_{-\beta} + (\alpha-\delta|v|\gamma-\beta)\, a_\alpha^\dagger a_{-\delta}^\dagger a_\gamma a_{-\beta} + (\alpha-\delta|v|-\beta\gamma)\, a_\alpha^\dagger a_{-\delta}^\dagger a_{-\beta} a_\gamma\Big\}.$$

Using the symmetry of v and the anticommutation rules of the creation and annihilation operators, we may reduce this to

$$\big[(-\delta\alpha|v|\gamma-\beta) - (-\delta\alpha|v|-\beta\gamma)\big]\, a_{-\delta}^\dagger a_\alpha^\dagger a_\gamma a_{-\beta}.$$

From the phase convention chosen we obtain

$$\langle \bar\alpha\bar\beta|V|\bar\gamma\bar\delta\rangle = (-1)^{(j_\beta - m_\beta)+(\frac{1}{2}-m_{t\beta})+(j_\delta-m_\delta)+(\frac{1}{2}-m_{t\delta})+1}\big[(-\delta\alpha|v|\gamma-\beta)-(-\delta\alpha|v|-\beta\gamma)\big]$$

$$= (-1)^{(j_\beta-j_\delta)+(m_\beta-m_\delta)+(m_{t\beta}-m_{t\delta})}\big[(-\delta\alpha|v|-\beta\gamma)-(-\delta\alpha|v|\gamma-\beta)\big].$$

Thus we obtain

$$\langle(\bar\alpha\bar\beta)\,JMTM_T|V|(\bar\gamma\bar\delta)\,JMTM_T\rangle = \sum_{m's,\, m_t's} (j_\alpha m_\alpha j_\beta m_\beta | JM)(j_\gamma m_\gamma j_\delta m_\delta | JM)$$

$$\times (\tfrac{1}{2} m_{t\alpha} \tfrac{1}{2} m_{t\beta} | TM_T)(\tfrac{1}{2} m_{t\gamma} \tfrac{1}{2} m_{t\delta} | TM_T)\,(-1)^{j_\beta - j_\delta + m_\beta - m_\delta + m_{t\beta} - m_{t\delta}}$$

$$\times \Big\{(n_\delta l_\delta j_\delta - m_\delta - m_{t\delta};\ n_\alpha l_\alpha j_\alpha m_\alpha m_{t\alpha}|v|n_\beta l_\beta j_\beta - m_\beta - m_{t\beta};\ n_\gamma l_\gamma j_\gamma m_\gamma m_{t\gamma})$$

$$- (n_\delta l_\delta j_\delta - m_\delta - m_{t\delta};\ n_\alpha l_\alpha j_\alpha m_\alpha m_{t\alpha}|v|n_\gamma l_\gamma j_\gamma m_\gamma m_{t\gamma};\ n_\beta l_\beta j_\beta - m_\beta - m_{t\beta})\Big\}. \quad (A.1)$$

We are now dealing with particle functions only. This is the result given in equation 17 of Lewis and Walecka (1964). The apparent difference of a factor -1 arises because they have used the convention

$$(ab|v|cd) = \int d\vec{x}_2 \int d\vec{x}_1 \, \psi_a^{\dagger}(\vec{x}_1) \, \psi_b^{\dagger}(\vec{x}_2) \, v(\vec{x}_1, \vec{x}_2) \, \psi_c(\vec{x}_1) \, \psi_d(\vec{x}_2) \, .$$

We may recouple the angular momenta in equation A.1 to obtain a more manageable expression. Since the procedures are the same for isotopic spin as for angular momentum, recoupling will be shown for the angular momentum only.

It is assumed that v does not depend upon the orientation of the system, so that the values of the matrix elements $((\alpha\beta)JM|v|(\gamma\delta)JM)$ do not depend upon the value of M. Then we may write

$$\langle(\alpha\beta)JM|V|(\gamma\delta)JM\rangle = (2J+1)^{-1} \sum_{M'} \langle(\alpha\beta)JM'|V|(\gamma\delta)JM'\rangle$$

$$= -(2J+1)^{-1} \sum_{M'} \sum_{m_\alpha, m_\gamma} (-1)^{j_\beta - m_\beta + j_\delta - m_\delta} (j_\alpha m_\alpha j_\beta M'-m_\alpha | JM')(j_\gamma m_\gamma j_\delta M'-m_\gamma | JM')$$

$$\times \left\{ (j_\alpha m_\alpha ; j_\delta - M'+m_\gamma | v | j_\beta - M'+m_\alpha ; j_\gamma + m_\gamma) - (j_\alpha + m_\alpha ; j_\delta - M'+m_\gamma | v | j_\gamma + m_\gamma ; j_\beta - M'+m_\alpha) \right\} \quad \text{(A.2)}$$

From equation 6.2.6 of Edmonds (1960) and from the properties of Clebsch-Gordan coefficients, we have a relationship

$$(-1)^{j_2 - m_2 + j_4 - m_4} (j_1 m_1 j_2 M-m_1 | JM)(j_3 m_3 j_4 M-m_3 | JM) = (2J+1) \sum_{J'} \begin{Bmatrix} j_1 & j_2 & J \\ j_3 & j_4 & J' \end{Bmatrix}$$

$$\times (j_1 + m_1 \, j_4 - M+m_3 \, | \, J'-M+m_1+m_3)(j_3 + m_3 \, j_2 - M+m_1 \, | \, J'-M+m_1+m_3) \, . \quad \text{(A.3)}$$

Applying this equation we obtain

$$\langle(\alpha\beta)JM'|V|(\gamma\delta)JM'\rangle = -\sum_{J'} \begin{Bmatrix} j_\alpha & j_\beta & J \\ j_\gamma & j_\delta & J' \end{Bmatrix} \sum_{M', m_\alpha, m_\gamma} (j_\alpha + m_\alpha \, j_\delta - M'+m_\gamma \, | \, J'-M+m_\alpha+m_\gamma)$$

$$\times (j_\gamma + m_\gamma \, j_\beta - M'+m_\alpha \, | \, J'-M'+m_\gamma+m_\alpha) \left\{ (j_\alpha - m_\alpha ; j_\delta - M'+m_\gamma | v | j_\beta - M'+m_\alpha ; j_\gamma + m_\gamma) \right.$$

$$\left. - (j_\alpha + m_\alpha ; j_\delta - M'+m_\gamma | v | j_\gamma + m_\gamma ; j_\beta - M'+m_\alpha) \right\} . \quad \text{(A.4)}$$

We may replace the dummy index of summation M' by $-M''+m_\alpha+m_\gamma$. This gives

$$\langle(\alpha\bar{\beta})JM'|V|(\gamma\bar{\delta})JM'\rangle = -\sum_{J'}\begin{Bmatrix} j_\alpha & j_\beta & J \\ j_\gamma & j_\delta & J' \end{Bmatrix}\sum_{M'',m_\alpha,m_\gamma}(j_\alpha+m_\alpha\, j_\delta-M''+m_\alpha|J'M'')$$

$$\times(j_\gamma+m_\gamma\, j_\beta\, M''-m_\gamma|J'M'')\left\{(j_\alpha+m_\alpha; j_\delta\, M''-m_\alpha|v|j_\beta\, M''-m_\gamma; j_\gamma+m_\gamma)\right.$$

$$\left.-(j_\alpha+m_\alpha; j_\delta\, M''-m_\alpha|v|j_\gamma+m_\gamma\, j_\beta\, M''-m_\gamma)\right\}$$

$$=-\sum_{J'}\begin{Bmatrix} j_\alpha & j_\beta & J \\ j_\gamma & j_\delta & J' \end{Bmatrix}\sum_{M''}\left\{((j_\alpha j_\delta)J'M''|v|(j_\beta j_\gamma)J'M'')\right.$$

$$\left.-(-1)^{j_\gamma+j_\beta-J'}((j_\alpha j_\delta)J'M''|v|(j_\gamma j_\beta)J'M'')\right\}$$

$$=-\sum_{J'}\begin{Bmatrix} j_\alpha & j_\beta & J \\ j_\gamma & j_\delta & J' \end{Bmatrix}(2J'+1)\left[((j_\alpha j_\delta)J'M'|v|(j_\beta j_\gamma)J'M')\right.$$

$$\left.-(-1)^{j_\gamma+j_\beta-J'}((j_\alpha j_\delta)J'M'|v|(j_\gamma j_\beta)J'M')\right]. \qquad \text{(A.5)}$$

The order in which α, β, γ, and δ appear in equation A.5 indicates the method by which the integration is to be carried out. The integration convention is given following equation 2.5.

APPENDIX B

REDUCTION OF ISOTOPIC SPIN TERMS

The multipole operators may be factored to give operators of the form $N^{o}_{\lambda}\left[\frac{1}{2}(n_o+n_1\tau_3)\right]$, where N^{o}_{λ} operates on spin and orbital angular momenta. We consider the matrix element $\left((\alpha\bar{\beta})\lambda 0\, T0\,|N^{o}_{\lambda}\left[\frac{1}{2}(n_o+n_1\tau_3)\right]|\,g\right)$.

When T = 0, only the scalar part of the isotopic spin operator ($\frac{1}{2}n_o$) can form a vector triangle in isotopic spin space with the initial and final state vectors. Similarly for T = 1, only the isovector part of the operator ($\frac{1}{2}n_1\tau_3$) need be considered. The n_o and n_1 are related to the corresponding quantities for neutron and proton by $n_o = n_p + n_n$ and $n_1 = n_p - n_n$.

Let us consider the case when T = 1, making use of creation and annihilation operators.

$$\left\langle(\alpha\bar{\beta})\lambda 010\,|N^{o}_{\lambda}\left[\tfrac{1}{2}(n_o+n_1\tau_3)\right]|\,g\right\rangle = \sum_{\substack{m,\bar{m}\\ m_t,\bar{m}_t}}\left(j_\alpha m\, j_\beta -\bar{m}\,|\lambda 0\right)\left(\tfrac{1}{2}\,m_t\,\tfrac{1}{2}-\bar{m}_t\,|10\right)$$

$$\times\left\langle n_\alpha \ell_\alpha j_\alpha\, m\, m_t;\ \bar{n}_\beta \bar{\ell}_\beta \bar{j}_\beta -\bar{m}\,-\bar{m}_t\,|N^{o}_{\lambda}\tfrac{1}{2}n_1\tau_3\,|\,g\right\rangle .$$

For convenience we write $|\alpha,-\bar{\beta}\rangle$ for $|n_\alpha \ell_\alpha j_\alpha\, m m_t;\ \bar{n}_\beta \bar{\ell}_\beta \bar{j}_\beta -\bar{m}-\bar{m}_t\rangle$.

Now

$$a_\beta\,|g\rangle = (-1)^{j_\beta+\bar{m}+\frac{1}{2}+\bar{m}_t}\,|-\bar{\beta}\rangle \quad \text{or} \quad |-\bar{\beta}\rangle = (-1)^{j_\beta+\bar{m}+\frac{1}{2}+\bar{m}_t}\,a_\beta\,|g\rangle .$$

The state $|-\bar{\beta}\rangle$ has an odd number of occupied states below the state α.

Therefore

$$a^{\dagger}_{\alpha}\,|-\bar{\beta}\rangle = (-1)^{1}\,|\alpha,-\bar{\beta}\rangle \text{ and so}$$

$$|\alpha,-\bar{\beta}\rangle = (-1)^{j_\beta+\bar{m}+\frac{1}{2}+\bar{m}_t+1}\;a^{\dagger}_{\alpha}a_\beta\,|g\rangle$$

We have

$$\left\langle(\alpha\bar{\beta})\lambda 010\,|N^{o}_{\lambda}\left[\tfrac{1}{2}(n_o+n_1\tau_3)\right]|\,g\right\rangle = \sum_{\gamma,\delta}\sum_{\substack{m,\bar{m}\\ m_t,\bar{m}_t}}(-1)^{j_\beta+\bar{m}+\frac{1}{2}+\bar{m}_t+1}\left(j_\alpha m\, j_\beta -\bar{m}\,|\lambda 0\right)$$

$$\times\left(\tfrac{1}{2}\,m_t\,\tfrac{1}{2}-\bar{m}_t\,|10\right)\left\langle g\,|\,a^{\dagger}_{\beta}a_\alpha\,a^{\dagger}_{\gamma}a_\delta\,|\,g\right\rangle\left(\gamma\,|N^{o}_{\lambda}\tfrac{1}{2}n_1\tau_3\,|\,\delta\right)$$

$$= \sum_{\substack{m,\bar{m}\\ m_t,\bar{m}_t}} (-1)^{j_\beta+\bar{m}-2\bar{m}+(2\bar{m}+1)+\frac{1}{2}+\bar{m}_t} \left(j_\alpha m\, j_\beta -\bar{m} \,|\lambda 0\right)\left(\tfrac{1}{2} m_t\, \tfrac{1}{2} -\bar{m}_t |10\right)\left(\alpha \left| N^\circ_\lambda \tfrac{1}{2} n_1 \tau_3 \right| \beta\right)$$

$$= \sum_{m,\bar{m}} (-1)^{j_\beta-\bar{m}} \left(j_\alpha m\, j_\beta -\bar{m}\,|\lambda 0\right)\left(n_\alpha l_\alpha j_\alpha m\right| N^\circ_\lambda \left| n_\beta l_\beta j_\beta \bar{m}\right) \sum_{m_t,\bar{m}_t} (-1)^{\frac{1}{2}+\bar{m}_t} \left(\tfrac{1}{2} m_t\, \tfrac{1}{2} -\bar{m}_t |10\right)$$

$$\times \left(m_t \left| \tfrac{1}{2} n_1 \tau_3 \right| \bar{m}_t\right)$$

$$= \frac{(\alpha \| N_\lambda \| \beta)}{\sqrt{2\lambda+1}} \left\{(-1)^1 \left(\tfrac{1}{2}\tfrac{1}{2}\tfrac{1}{2} -\tfrac{1}{2}|10\right)\left(\tfrac{1}{2}\left|\tfrac{1}{2} n_1 \tau_3\right|\tfrac{1}{2}\right) + (-1)^0 \left(\tfrac{1}{2} -\tfrac{1}{2}\tfrac{1}{2}\tfrac{1}{2}|10\right)\left(-\tfrac{1}{2}\left|\tfrac{1}{2} n_1 \tau_3\right|-\tfrac{1}{2}\right)\right\}$$

by equation 5.4.2 of Edmonds (1960). The result is

$$\left\langle (\alpha\bar{\beta})\lambda 010 \left| N^\circ_\lambda \left[\tfrac{1}{2}(n_\circ + n_1\tau_3)\right]\right| g\right\rangle = -\frac{(\alpha \| N^\circ_\lambda \| \beta)}{\sqrt{2\lambda+1}} \frac{n_1}{\sqrt{2}} . \qquad \text{(B.1)}$$

In a similar manner we obtain for T = 0

$$\left\langle (\alpha\bar{\beta})\lambda 000 \left| N^\circ_\lambda \left[\tfrac{1}{2}(n_\circ + n_1\tau)\right]\right| g\right\rangle = -\frac{(\alpha \| N^\circ_\lambda \| \beta)}{\sqrt{2\lambda+1}} \frac{n_\circ}{\sqrt{2}} . \qquad \text{(B.2)}$$

Jolly (1964) gives this result to within a factor (-1). The difference is due to slightly different methods of defining the states $|(\alpha\bar{\beta})\lambda 0 T 0\rangle$ Jolly did not include a factor $(-1)^1$ for the $a^\dagger_-$ operating on the state $|-\bar{\beta}\rangle$ (Jolly (1964), equation 3.1). Since cross sections are not changed if all amplitudes are multiplied by (-1), the different methods of defining particle-hole states give the same electron scattering cross sections.

APPENDIX C

DETECTOR DEAD TIME LOSSES

If both sides of equation 4.2 are divided by the number of electrons reaching the target per unit time, the result is an expression for the probability that an electron will be scattered and will reach the detector. The probability

$$\pi = \frac{d^2\sigma}{d\Omega\, dE_f}\,\Delta\Omega\,\Delta E_f N_t \tag{C.1}$$

is very small. The scattering of an electron into the detector can be considered to be a random process. If n electrons strike the target per pulse, the probability that exactly p of them reach the detector during a pulse is given be the binomial distribution

$$Pr\{p\} = \binom{n}{p}\pi^p(1-\pi)^{n-p}. \tag{C.2}$$

When n is very large and π very small, the binomial distribution may be approximated by the Poisson distribution

$$Pr\{p\} = e^{-\pi n}\frac{(\pi n)^p}{p!} = e^{-\bar{p}}\frac{(\bar{p})^p}{p!}, \tag{C.3}$$

where $\bar{p} = \pi n$ is the average number of electrons scattered into the detector per pulse.

We now suppose that the detection system is capable of registering not more than 1 count per pulse. The average counting rate with such a detector is

$$\bar{r} = 0\times Pr\{0\} + 1\times Pr\{1\} + 1\times Pr\{2\} + \ldots = \sum_{i=1} e^{-\bar{p}}\frac{\bar{p}^i}{i!} = 1 - exp(-\bar{p}). \tag{C.4}$$

In this case the variance in r is simply

$$\sigma_r^2 = e^{-\bar{p}}(1-e^{-\bar{p}}) = (1-\bar{r})\bar{r}. \tag{C.5}$$

σ_r^2 is the variance in the value obtained for one pulse. But measurements are made over a large number of pulses. What we want to know is the

variance in average counting rates when the averaging is done over a large number of pulses. By the central limit theorem we know that when $\bar{r}$ is averaged over K pulses and when K is a large number, then the distribution of $\bar{r}$ is Gaussian and that the variance in $\bar{r}$ is 1/K times the variance in r, that is

$$\sigma_{\bar{r}}^2 = \frac{e^{-\bar{p}}(1-e^{-\bar{p}})}{K} . \qquad (C.6)$$

(See, for example, Mathews and Walker (1964), page 360.)

If $\sigma_{\bar{r}}$ is small, the values of $\bar{p}$ calculated from counting rates will have a standard deviation $\sigma_{\bar{p}} = \frac{d\bar{p}}{d\bar{r}} \sigma_{\bar{r}}$, that is, we may replace the curve of $\bar{p}$ vs. $\bar{r}$ by its slope at a particular point. We get

$$\sigma_{\bar{p}} = \frac{d\bar{p}}{d\bar{r}} \sigma_{\bar{r}} = \sqrt{\frac{e^{\bar{p}}-1}{K}} = \sqrt{\frac{\bar{r}}{K(1-\bar{r})}} . \qquad (C.7)$$

We want to minimize the ratio of standard deviation to average value of $\bar{p}$. This quantity, as a function of $\bar{r}$, is

$$\frac{\sigma_{\bar{p}}}{\bar{p}} = \sqrt{\frac{\bar{r}}{K(1-\bar{r})}} \Big/ \ln\left(\frac{1}{1-\bar{r}}\right) . \qquad (C.8)$$

This quantity is plotted in figure C.1. The ratio for a detector with no dead time losses is also shown. We see that for a detection system which gives not more than one count per pulse there is the following rule: choose beam current so as to give the highest possible counting rate, provided that this does not exceed $\bar{r} = 0.8$ per pulse.

Several implicit assumptions have been made in obtaining this rule. They are:

1) n, the number of electrons striking the target per pulse, does not vary from pulse to pulse.

2) The detector efficiency is 1.0, that is, the first electron reaching the detector during a pulse is always counted.

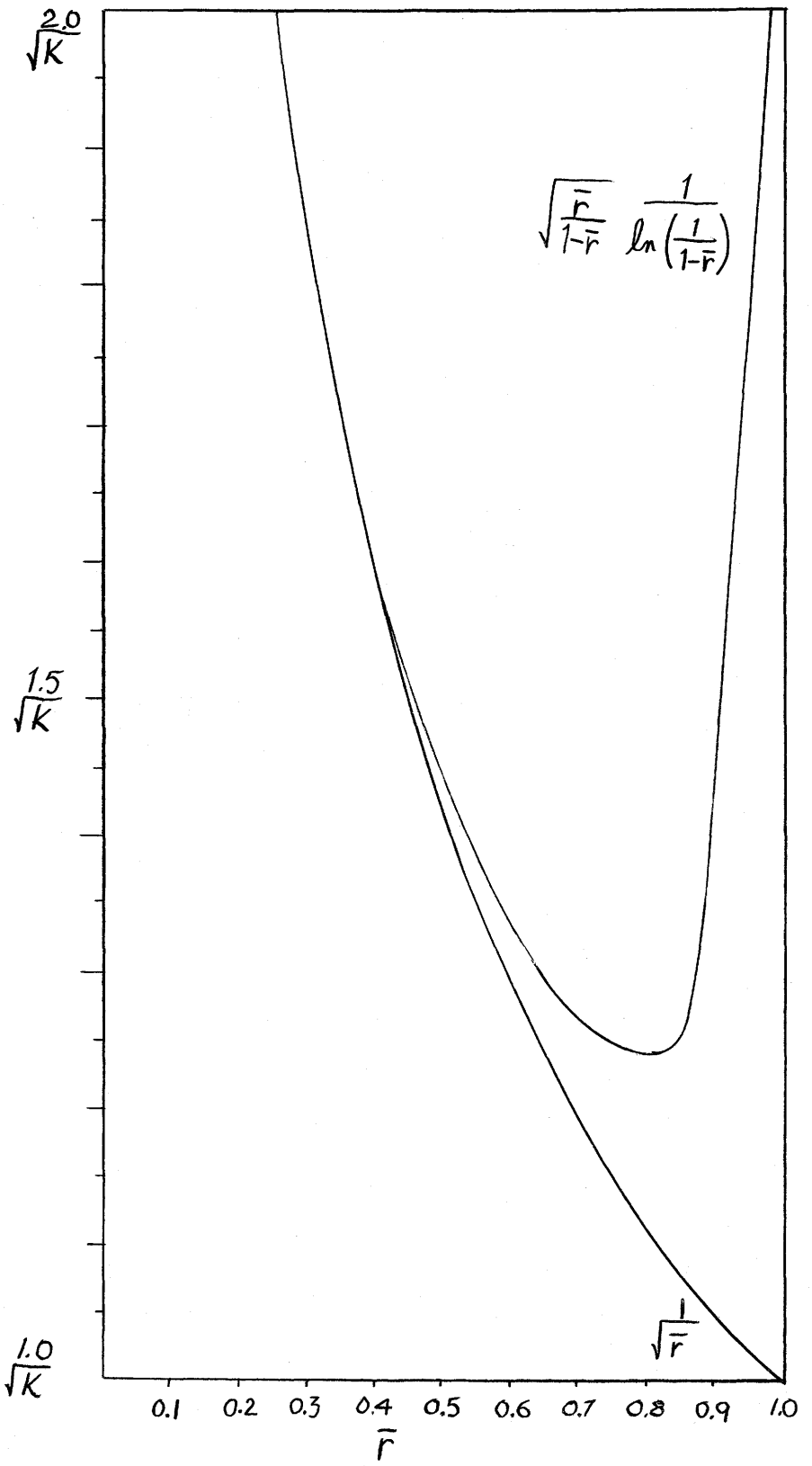

Fig. C.1 $\sigma_{\bar{p}}/\bar{p}$ vs. $\bar{p}$ with and without detector dead time.

3) Any background is proportional to n, so the ratio of background to signal counting rates remains constant.

If there is a constant background present, the optimum counting rate is increased somewhat. Suppose that a source of background causes particles to reach the detector at an average rate of $\bar{a}$ per pulse with variance $\sigma_a^2 = \bar{a}$. If the scattering process which is being studied gives an average rate of $\bar{p}$ particles per pulse at the detector, there are on the average $\bar{s} = \bar{p} + \bar{a}$ particles reaching the detector per pulse. We again wish to minimize $\sigma_{\bar{p}}/\bar{p}$. Making use of the fact that $\sigma_{\bar{p}}^2 = \sigma_{\bar{s}}^2 + \sigma_{\bar{a}}^2$ and obtaining $\sigma_{\bar{s}}^2$ in the same method as $\sigma_{\bar{p}}^2$ was obtained above, we get

$$\frac{\sigma_{\bar{p}}}{\bar{p}} = \frac{\sqrt{\frac{1}{K}\left(e^{\bar{s}} - 1 + \bar{a}\right)}}{\bar{s} - \bar{a}} = \frac{\sqrt{\frac{1}{K}\left(\frac{\bar{t}}{1-\bar{t}} + \bar{a}\right)}}{\ln\left(\frac{1}{1-\bar{t}}\right) - \bar{a}}, \qquad \text{(C.9)}$$

where $\bar{t}$ is the observed counting rate.

LIST OF REFERENCES

Ajzenberg-Selove, F. and Lauritsen, T. 1959. Nuclear Physics 11, 1.

Barber, W.C. 1962. Annual Review of Nuclear Science 12, 1.

Barber, W.C., Berthold, F., Fricke, G., and Gudden, G.E. 1960. Physical Review 120, 2081.

Beer, G.A. 1964. Saskatchewan Accelerator Laboratory, Internal Report No. 11.

Bell, J.S. 1959. Nuclear Physics 12, 117.

Bethe, H.A. and Ashkin, J. 1953. in Experimental Nuclear Physics Vol. 1, edited by E. Segrè (John Wiley and Sons, Inc., New York).

Bizzeti, P.G., Bizzeti Sona, A.M., Bocciolini, M., DiCaporiacco, G., Fazzini, T., and Mandò, M. 1965. Nuclear Physics 63, 161.

Bounin, P. and Bishop, G.R. 1961. Le Journal de Physique et le Radium 22, 555.

Brown, G.E. and Bolsterli, M. 1959. Physical Review Letters 3, 472.

Cannington, P.H., Stewart, R.J.J., Hogg, G.R., Lokan, K.H., and Sargood, D.G. 1965. University of Melbourne, Report UM-P-65/7.

Edmonds, A.R. 1960. Angular Momentum in Quantum Mechanics, 2nd edition (Princeton University Press, Princeton).

Elliot, J.P. and Lane, A.M. 1957. in Handbuch der Physik, Vol. 39, edited by S. Flügge (Springer-Verlag, Berlin).

Elliott, R.V. 1964. M.Sc. Thesis, University of Saskatchewan.

Ericson, T. 1963. in Rendiconti della Scuola Internazionale di Fisica «Enrico Fermi» XXIII Corso (Academic Press, New York).

Gillet, V. 1962. Ph.D. Thesis, University of Paris.

Goldemberg, J. and Barber, W.C. 1964. Physical Review 134, B963.

Heitler, W. 1954. The Quantum Theory of Radiation, 3rd ed. (Clarendon Press, London).

Helm, R.H. 1956. Physical Review 104, 1466.

Hofstadter, R. 1957. Annual Review of Nuclear Science 7, 231.

Isabelle, D.B. and Bishop, G.R. 1963. Nuclear Physics 45, 209.

Jolly, H.P. 1964. Massachusetts Institute of Technology, Internal Report.

Leiss, J.E. and Taylor, R.E. 1960. in Contributions to the Karlsruhe Photonuclear Conference.

Lewis, F.H. Jr. 1964. Physical Review 134, B331.

Lewis, F.H. Jr. and Walecka, J.D. 1964. Physical Review 133, B849.

Maikov, V.N. 1958. JETP 7, 972.

Mathews, J. and Walker, R.L. 1964. Mathematical Methods of Physics (W.A. Benjamin, Inc., New York).

Matsonabu, H. and Takebe, H. 1955. Progress of Theoretical Physics 14, 589.

Maximon, L.C. and Isabelle, D.B. 1964. Physical Review 133, B1344.

Mayer, M.G. and Jensen, J.H.D. 1955. Elementary Theory of Nuclear Shell Structure (John Wiley and Sons, New York).

Nguyen Ngoc, H. and Perez y Jorba, J.P. 1964. Laboratoire de l'Accélérateur Linéaire, Report 1108.

Preston, M.A. 1962. Physics of the Nucleus (Addison-Wesley Publishing Co., Inc., Reading).

Reay, N.W., Hintz, N.M., and Lee, L.L. Jr. 1963. Nuclear Physics 44, 338.

Rossi, B. 1952. High Energy Particles (Prentice-Hall, Englewood Cliffs).

Schiff, L.I. 1952. Physical Review 87, 750.

Schweber, S.S. 1962. An Introduction to Relativistic Quantum Field Theory (Harper and Row, New York).

Seaborn, J.B. and Eisenberg, J.M. 1965. Nuclear Physics 63, 496.

deShalit, A. and Talmi, I. 1963. Nuclear Shell Theory (Academic Press, New York).

Singh, P.P., Segel, R.E., Meyer-Schützmeister, L., Hanna, S.S., and Allas, R.G. 1965. Nuclear Physics 65, 577.

Stovall, T., Goldemberg, J., Isabelle, D.B., and Vinciguerra, D. 1965. Laboratoire de l'Accélérateur Linéaire, Report 1133.

Sykes, D.H. 1965. Private communication.

Tanner, N.W., Thomas, G.C., and Earle, E.D. 1964. Nuclear Physics 52, 45.

Taran, G.G. and Gorbunov, A.N. 1964. JETP 19, 1010.

Tassie, L.J. 1957. Nuovo Cimento 5, 1497.

Titze, O. 1964. Diplomarbeit, Institut für Technische Kernphysik der Technischen Hochshule, Darmstadt.

Vanhuyse, V.J. and Barber, W.C. 1961. Nuclear Physics 26, 233.

Vanpraet, G. 1965. High Energy Physics Laboratory, Stanford, Report 365.

Vinh-Mau, N. and Brown, G.E. 1962. Nuclear Physics 29, 89.

Willey, R.S. 1963. Nuclear Physics 40, 529.

Yergin, P.F., Augustson, R.H., Kaushal, N.N., Medicus, H.A., Moyer, W.R., and Winhold, E.J. 1964. Physical Review Letters 12, 733.